



HAL
open science

Common features in the thermoacoustics of flames and engines

Chris J Lawn, Guillaume Penelet

► **To cite this version:**

Chris J Lawn, Guillaume Penelet. Common features in the thermoacoustics of flames and engines. *International Journal of Spray and Combustion Dynamics* , 2017, 10 (1), pp.3 - 37. 10.1177/1756827717743911 . hal-01877680

HAL Id: hal-01877680

<https://univ-lemans.hal.science/hal-01877680>

Submitted on 20 Sep 2018

HAL is a multi-disciplinary open access archive for the deposit and dissemination of scientific research documents, whether they are published or not. The documents may come from teaching and research institutions in France or abroad, or from public or private research centers.

L'archive ouverte pluridisciplinaire **HAL**, est destinée au dépôt et à la diffusion de documents scientifiques de niveau recherche, publiés ou non, émanant des établissements d'enseignement et de recherche français ou étrangers, des laboratoires publics ou privés.

Common features in the thermoacoustics of flames and engines

Chris J Lawn¹ and Guillaume Penelet²

Abstract

Thermoacoustic phenomena generated inadvertently during combustion, and those produced by heating and cooling material to generate a temperature gradient, have mostly been studied independently. Indeed, researchers of one phenomenon are seldom familiar with the literature on the other. This paper seeks to remedy this by reviewing the two subjects alongside one another, by comparing and contrasting them where possible. There is a brief account of the historically important papers in the development of both subjects, followed by a description of the nature of the phenomena. A selective number of papers is called upon to illustrate these principles. Techniques for handling the pure acoustics in the two subjects are addressed, before an outline is given of the modelling of the two thermoacoustic systems. Non-linear phenomena in the two systems are then explored. Finally, methods of ‘control’, of changing the system characteristics, are briefly discussed.

Keywords

Thermoacoustics, combustion instability, unsteady heat transfer, non-linear response, Rijke tubes

Date received: 27 June 2017; accepted: 29 October 2017

1. Introduction: History of thermoacoustics and the range of phenomena

1.1 A brief history of thermoacoustics (the early years)

The first published account of a thermoacoustic phenomenon is usually attributed to one Byron Higgins,¹ whose work of 1777 was recorded in 1802 in *J Phil Chem Arts*. He burnt hydrogen in a tube to produce what we now call ‘a singing flame’. However, Ueda² reported in a workshop that a thermoacoustic device, the ‘Kibitsunokama’, was mentioned in the diary of a Buddhist monk in 1568. In this device,

a barrel is mounted on an iron bowl and both its ends are open. A woody mesh screen is located in the barrel and covered with rice grains, and liquid water is placed in the iron bowl. When the water is externally heated, the gas in the Kibitsunokama begins to oscillate spontaneously and emits a sound similar to the lowing of cattle; this sound is used in fortune telling.

Ueda then demonstrated the phenomenon in the workshop.

Moreover, it is said that sound emission was regularly experienced by glass blowers when heating a bulb of gas joined to a cooler tube (Figure 1(a)). This was investigated by Sondhauss,³ but there was reference to the effect in 1804 and the experience may even have pre-dated Higgin’s observations on the singing flame. Thus, the first thermoacoustic experiences were probably flameless. Somewhat later, another process similar to the Sondhauss effect (but with a cold source) was observed in cryogenic experiments when the open end of a tube was immersed in liquid helium.⁴

A tube open at both ends with a thermal perturbation about a quarter of the way along it (Figure 1(b) and (c)) to create a standing wave, as in the singing flame, is an example of a ‘Rijke’ tube. A version with

¹School of Engineering and Materials Science, Queen Mary University of London, London, UK

²Laboratoire d’Acoustique, de l’Université du Maine, Le Mans Cedex, France

Corresponding author:

Chris J Lawn, Queen Mary University of London, Mile End Rd, London E1 4NS, UK.

Email: c.j.lawn@qmul.ac.uk



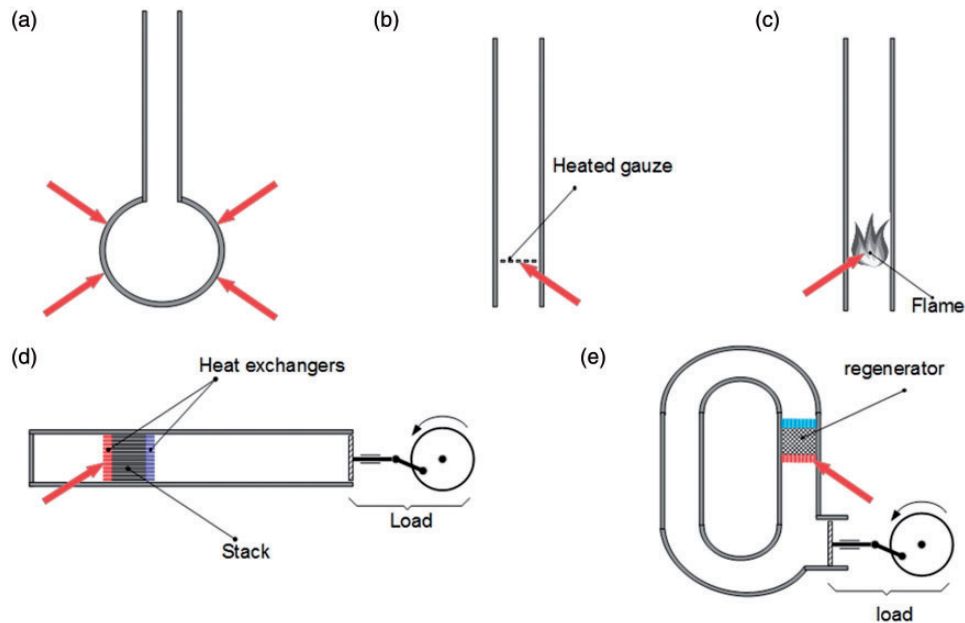


Figure 1. (a) Sondhauss tube, with a heated bulb; (b) Rijke tube with a heated gauze; (c) Rijke tube with a flame; (d) thermoacoustic standing-wave prime mover; (e) thermoacoustic travelling-wave prime mover.

a heated gauze was described in Rijke.⁵ This is the configuration in which the most obvious comparison between thermoacoustics with and without flames can be made.

1.2 Types of flame where acoustic excitation is encountered

While the singing flame can be regarded as something of a diverting curiosity, and indeed has been built into rudimentary musical instruments, thermoacoustic excitation of equipment by flames has become an issue of military and industrial importance.

This really began in the late 1930s and early 1940s with the development of so-called pulse combustors for missiles, in particular the V-1 buzz bombs. In such devices, the fuel supply may or may not be steady but the combustion chamber air pulses are controlled either by mechanical valves which shut with the build-up of pressure, or simply by the aerodynamic characteristics of the chamber which allows expansion more easily in one direction. This is a combustion-induced oscillation in which the fundamental longitudinal acoustic mode of the system is excited.⁶

Much higher frequencies were experienced during the development of rockets for the space programme in the 1960s. With both solid and liquid fuels, modes corresponding to both the longitudinal and the transverse dimensions can be excited. Culick⁷ presents a comprehensive review of these phenomena.

While the gas turbines being developed for the burgeoning aircraft industry in the 1950s and 1960s were

largely immune from thermoacoustic problems, this was not true of the reheat (after-burner) systems. Kerosene fuel injected directly into the gas turbine exhaust is very susceptible to instabilities in the exhaust flow. Major advances in the quantitative description of thermoacoustics were made in tackling this problem by Dowling⁸ and her team.

In the 1950s, rather different combustion-induced oscillations excited interest when domestic and industrial gas boilers experienced vibration of the tubes and environmental noise nuisance. Developments involving the intensification of the combustion drove the equipment into a regime where the timescales of response in the flame were commensurate with the timescales of the primary acoustic modes so that these were spontaneously excited, in the 50–1000 Hz range.⁹ Where the burners were naturally aspirated, with air drawn in through jet pumps, the system was essentially the same as the Rijke tube.

Chiefly due to the longer timescales associated with the burning of residual fuel oil (RFO) and coal, thermoacoustic problems in large power station boilers were comparatively rare, but not unknown, in this period. However, with the intensification of the combustion process, at least one design of RFO boiler experienced major difficulty in reaching full power during commissioning in the early 1980s because of the combustion-induced vibration of the boiler tubes.¹⁰ In this case, the divided furnace chamber resonated with the two sides in anti-phase, bringing the frequency down to 11–12 Hz. This was excited by periodic extinction and re-ignition of the central core of the flames.

This mechanism is also one of those now encountered in the large gas turbines that have been developed since the early 1990s for ‘industrial’, land-based use. So severe have been the problems associated with burning natural gas in the lean-burn mode to suppress NO_x that there has been an enormous explosion of scientific effort on thermoacoustic phenomena generally. Many other mechanisms of excitation have been identified (see Section 2.2) and there are many different types of combustion chamber.¹¹ In the last 10 years, major advances in understanding have been made particularly in exploring non-linear processes leading to limit cycling. A premixed combustor for a gas turbine is shown schematically in Figure 2.

1.3. Thermoacoustic engines: Prime movers and refrigerators

Although thermoacoustic excitation in devices such as the Kibitsunokama, Sondhauss tube and Rijke tube were clearly investigated much earlier, there do not appear any serious attempts to design a prime mover based on this acoustic energy until the pioneering work of Ceperley,¹³ and the research initiated at Los Alamos National Laboratory by Wheatley and his collaborators in the early 1980s. The earlier devices essentially involved an acoustic resonator equipped with a short (compared to the wavelength) stack of plates subjected to a temperature gradient by means of two heat exchangers. This kind of device will be referred to as a stack-based standing wave engine in the following. It can either be a prime-mover (generation of thermoacoustic oscillations due to the maintenance of a temperature gradient along the stack) or a heat pump (heat

transport along the stack promoted by the maintenance of sound).

As an example, the standing wave prime-mover built in the early history of thermoacoustic engines by Swift¹⁴ can deliver up to 700 W of acoustic energy to its load, with a thermal efficiency of 9% (13% relative to Carnot’s efficiency). This device, which is illustrated schematically in Figure 1(d), consists of a cylindrical resonator filled with 13.8 bar helium. As pointed out very early by Wheatley et al.,¹⁵ stack-based thermoacoustic engines involve a thermodynamic process which is *intrinsically irreversible* – the spacing between the plates of the stack must be adjusted to ensure an *imperfect* thermal contact between the oscillating gas and the solid, which is a necessary condition to provide the suitable phasing between the gas motion and the temperature fluctuations.

It is, however, possible to design another class of thermoacoustic engine based on Ceperley’s concept,¹³ which itself was directly inspired by Stirling engines. These engines had been used since 1816. These are low frequency, high intensity devices, involving the movement of ‘displacers’, so they can hardly be described as ‘acoustic’. However, engines based on Ceperley’s concept dispense with the mechanical displacer and work in the 50–100 Hz range. Designing a thermoacoustic-Stirling engine (sometimes called a travelling wave engine) involves, firstly, replacing the stack by a regenerator (usually a matrix of finely divided material) to ensure a quasi-isothermal thermal contact with the fluid and, second, designing the acoustical network around the regenerator in such a way that pressure and velocity oscillate in phase, at least within the regenerator where work production occurs.

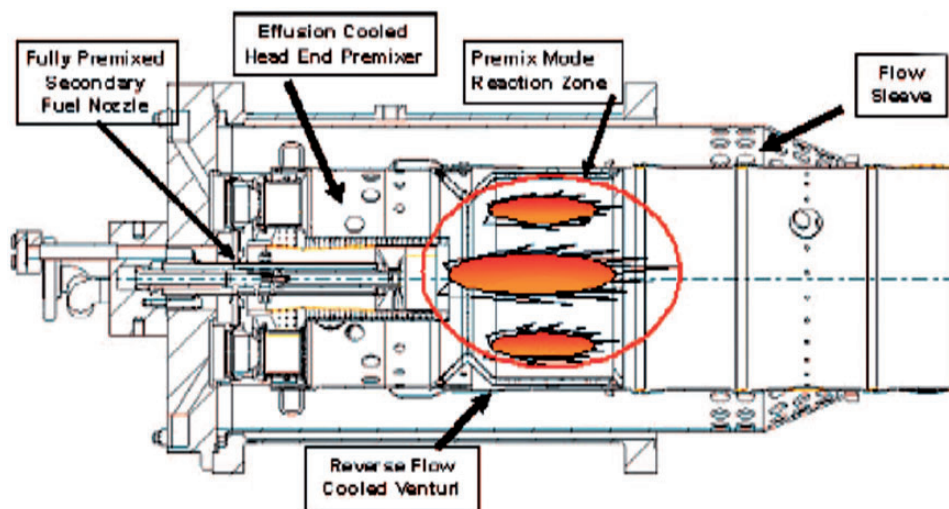


Figure 2. Axial vane gas turbine burner from Benoit et al.,¹² reproduced with the permission of the American Society of Mechanical Engineers.

As pointed out by Ceperley, this latter condition can be achieved by using a closed-loop resonator whose first resonance corresponds to a travelling wave rotating along the loop (Figure 1(e)); however, he failed to build this engine. The first experimental demonstration of a closed-loop travelling wave (but stack-based) thermoacoustic prime-mover is due to Yazaki et al.¹⁶

The first experimental demonstration of a thermoacoustic Stirling engine is presented in Figure 3: it was realised by Backhaus and Swift¹⁷ and achieved an efficiency of up to 24% based on power delivered to the load relative to the thermal input. The device also relies on the use of a closed-loop but its length is much shorter than the wavelength, while the working frequency is mainly determined by the load. Here, there is a quarter-wavelength resonator equipped with a dissipative load, but a linear alternator can be used instead (e.g. Backhaus et al.,¹⁸ who also achieved 24%). The loop actually provides an acoustical feedback which allows the appropriate phasing between pressure

and velocity in the regenerator, as well as an acoustic impedance which is much larger than that of a travelling wave to avoid viscous losses. This so-called ‘thermoacoustic Stirling heat engine’ (TASHE) design, which was developed by Tijani and Spoelstra¹⁹ to achieve 49% Carnot efficiency based on generating 280 W when filled with helium at 40 bar, has been the basis of many prime mover designs in the 21st century. (However, the maximum dissipation in the load was only 36 W in these experiments.) Another approach to designing the acoustical network and the coupling with the load to ensure an optimum process of thermoacoustic conversion in the regenerator is that of Yu et al.,²⁰ shown in Figure 4.

It should be appreciated that the above classification between stack-based standing wave engines and regenerator-based travelling wave engines is more or less artificial, since several existing engines could be ‘placed’ in between these two classes, and since both types of engines share many common features, notably regarding the non-linear effects saturating wave amplification.

Although they were not explicitly identified as thermoacoustic systems at the time, refrigeration systems based on standing-waves were developed much earlier²¹ based on the work of Gifford and Longworth in 1959 (reviewed in 1964²²). A pulse-tube variant known as an ‘Orifice Pulse Tube Refrigerator’ (OPTR), extracts power thermoacoustically from the wave generated by a loudspeaker while removing thermal energy from a cold heat exchanger. More recently, the reverse of Stirling engine amplification has been exploited in potentially more efficient travelling-wave thermoacoustic refrigeration systems. Such systems involve an acoustic driver sustaining a high amplitude resonance, while the acoustical network either involves a closed-loop²³ or a coaxial geometry²⁴ which in both cases are designed so that heat is pumped thermoacoustically along the regenerator from the cold to the ambient heat exchanger through a Stirling cycle.

The practical implementation of these concepts was greatly advanced by the work at Los Alamos in the 1990s. Some refrigeration examples are described in the book by Swift²⁵ which remains the major reference work on thermoacoustics. The development work at Los Alamos and elsewhere was mostly undertaken with electrical heating elements built into the loop to form the hot heat exchanger. Practical implementation requires the heat source to be external, whether it is from the burning of fuel, from solar power, or from industrial waste heat. This introduces additional problems in the matching of the characteristics of the systems. However, developments aimed at exploiting the heat of wood-burning stoves used for cooking,²⁶ the waste heat of a 200 kW wood-drying unit,²⁷ and concentrated solar radiation,²⁸ among many others,

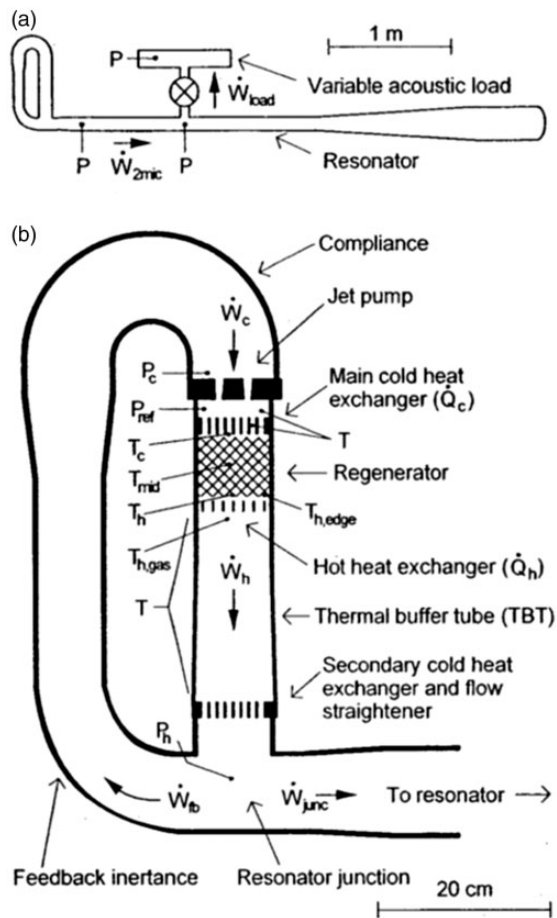


Figure 3. Thermoacoustic Stirling Heat Engine (TASHE) of Backhaus and Swift,¹⁷ reproduced with the permission of the Acoustical Society of America.

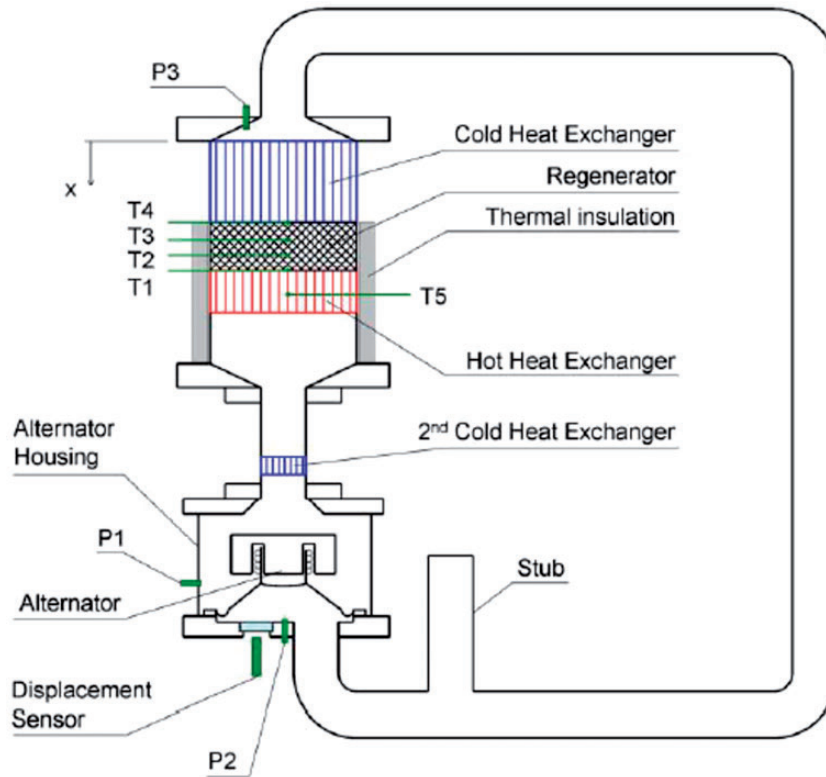


Figure 4. Thermoacoustic travelling-wave engine with a linear alternator in series, from Yu et al.,²⁰ reproduced with the permission of Sage Publications Ltd.

have been undertaken. Conversely, exploiting the cooling capability, a device has actually been flown on the Space Shuttle Discovery,²⁹ and industrially sized chillers have been installed,³⁰ although widespread introduction of refrigeration devices has not yet been achieved. The banning of HFCs from conventional refrigeration may open a future niche.

1.4 Structure of this comparative review

From this short survey, it will be apparent that research on the thermoacoustics of flames and on flameless engines has proceeded in parallel, but with little interrelation. It is the aim of this review to explore the similarities and differences of the two phenomena and to introduce researchers in each of the two fields to the methods used in the other. Only in the Rijke tube are the geometries and hence the acoustics essentially the same, so that the effect of the thermoacoustics can be isolated. However, there are many other points of similarity in the mathematical treatment of the phenomena.

Theory embracing both forms was produced by Lord Rayleigh³¹ and is the basis for the understanding of all thermoacoustic phenomena. This is discussed in Section 2.1 in this paper, before more detailed but still qualitative accounts of the mechanisms of excitation

are undertaken in Sections 2.2 and 2.3. There is then an exploration in Section 3 of the methods used to treat the acoustics of the two systems, with empirical data for the thermoacoustics, before methods to model the thermoacoustic mechanisms are outlined in Sections 4.1 and 4.2. The potential effects of gas composition and pressure are discussed in Section 4.3. Treatment of the Rijke tube in Section 4.4 is the precursor to discussion of the potential effects of non-linearity in Sections 4.5 to 4.7. Active and passive control methods are outlined in a final chapter in Section 5.

The strategy is not to provide a comprehensive review of the literature in the two fields, which would be an impossible task, but to use work familiar to the authors to outline the theoretical bases of the two and to compare and contrast them where possible.

2. Mechanisms of heat addition

2.1 The Rayleigh criterion

Essential for the understanding of all these thermoacoustic phenomena is an extension of the criterion enunciated by Rayleigh.³¹ The criterion expresses the fact that the flux of energy to the acoustic wave must be positive for the acoustic energy to grow.

With plane waves over a constant area incident upon the region of energy input, the energy equation for small perturbations may be written in the time domain

$$\bar{\rho}C_p \left\{ \frac{\partial T_a}{\partial t} + \bar{U} \frac{\partial T_a}{\partial x} + u \frac{\partial \bar{T}}{\partial x} \right\} = \frac{\partial p}{\partial t} + q \quad (1)$$

where T_a is the acoustic temperature fluctuation, p and u are the acoustic pressure and velocity, and q is the fluctuating component of heat transfer to the gas per unit volume. The over-bar denotes time-averaged, for velocity U , and temperature T . Invoking the continuity equation and the perfect gas law so as to convert fluctuations in density in that equation into those in temperature and pressure, and a low Mach number assumption to eliminate the mean velocity term, equation (1) may be translated to

$$\bar{\rho}C_p \bar{T} \frac{\partial u}{\partial x} = -\frac{\gamma}{\gamma-1} \frac{\partial p}{\partial t} + q + \frac{\partial p}{\partial t} = q - \frac{1}{\gamma-1} \frac{\partial p}{\partial t} \quad (2)$$

Given that the heat transfer zone is sufficiently thin in relation to the wavelength for the work done on the gas in compression and expansion to be negligible, this may be integrated to yield

$$\int q dx = \bar{\rho} \bar{T} C_p (u_d - u_u) \quad (3)$$

where subscript u denotes the incident wave and subscript d that exiting, as derived by Merk.³² The time-averaged gas properties can be evaluated anywhere in the region because their product $\bar{\rho} \bar{T} C_p$ is invariant for a perfect gas. Equation (3) expresses a change, not just in amplitude of the velocity fluctuations but also in their phase, due to the heat transfer. Consistent with the approximations leading to equation (3) is the simplification that the acoustic pressure is invariant in the flame region. Dowling³³ and Chen et al.³⁴ consider the changes across a moving flame front, including those in entropy fluctuations, in more detail.

The energy input to the acoustic wave is just the difference in acoustic powers $A \bar{p} \bar{u}$, exiting and entering the heat transfer region, where A is the cross-sectional flow area. From equation (3), the Rayleigh criterion is thus

$$\int \frac{\bar{p} \bar{q}}{C_p \bar{\rho} T} dV \equiv \frac{\gamma-1}{\bar{\rho} c^2} \int \bar{p} \bar{q} dV > 0 \quad (4)$$

where the integration is over the whole of the heat transfer domain. An extension of the Rayleigh criterion recognises that the criterion is necessary but not sufficient for acoustic growth, since every system has losses to be overcome.³⁵⁻³⁷ In the case of a flame in a Rijke

tube, the only substantial losses may be due to radiation from the ends of the tube. In the case of a swirl burner flame, it is likely that there are considerable losses in the air supply system and the swirler itself.

Considering energy transfer in the two regions away from the heat transfer zone leads to certain relationships between the acoustic impedance on the two sides of the region that must be satisfied for steady oscillations to occur at the eigen-frequencies.^{35,37} An alternative view is that the energy balance for the system as a whole determines the eigen-frequencies. The equations can only be solved if the heat transfer is related to some of the other acoustic variables, velocity or pressure.

2.2 Amplification in flames

In flames, this relation is known as the flame transfer function (FTF), a term first used by Merk,³² or more generally in the case of non-linearities, as the flame describing function (FDF). With a flow of combustible mixture through the flame zone, it is logical to relate the heat transfer into the gas (known almost universally as ‘the heat release rate’) to the upstream acoustic velocity. To compute the FTF, $\frac{q}{u_u}$, a model for the processes of flame disturbance is required.

Three separate mechanisms have been identified for premixed flames by numerous authors. They are described in detail in the book by Lieuwen.³⁸ The first two are also relevant to diffusion flames, while the third is replaced in that case by the changes of flame shape as the excess air fluctuates. These mechanisms are discussed in the context of a V-flame stabilised in the swirling flow generated by axial vanes (Figure 2). This is a common configuration in power station boilers and gas turbines. More processes are at work in other situations: a schematic diagram of the main possibilities is given as Figure 5.

1. *Acoustic velocity fluctuations at the flame front giving rise to kinematic perturbations in the position of the front, perturbations in area, and hence perturbations in heat release.* Overall, these occur with a time delay which is related to the convection velocities to the various parts of the flame front.
2. *Acoustic velocity fluctuations in the shear layers within and beyond the burner.* After transit to the front, these lead to propagation of the front relative to its steady position. The fluctuations at the front may also modify the burning velocity through the perturbations in turbulence intensity and length scale. Additionally, fluctuations within the burner may give rise to the shedding of discrete vortices, or to modulation of the swirl of the burner.⁴⁰ After a delay for their transit to the flame front,

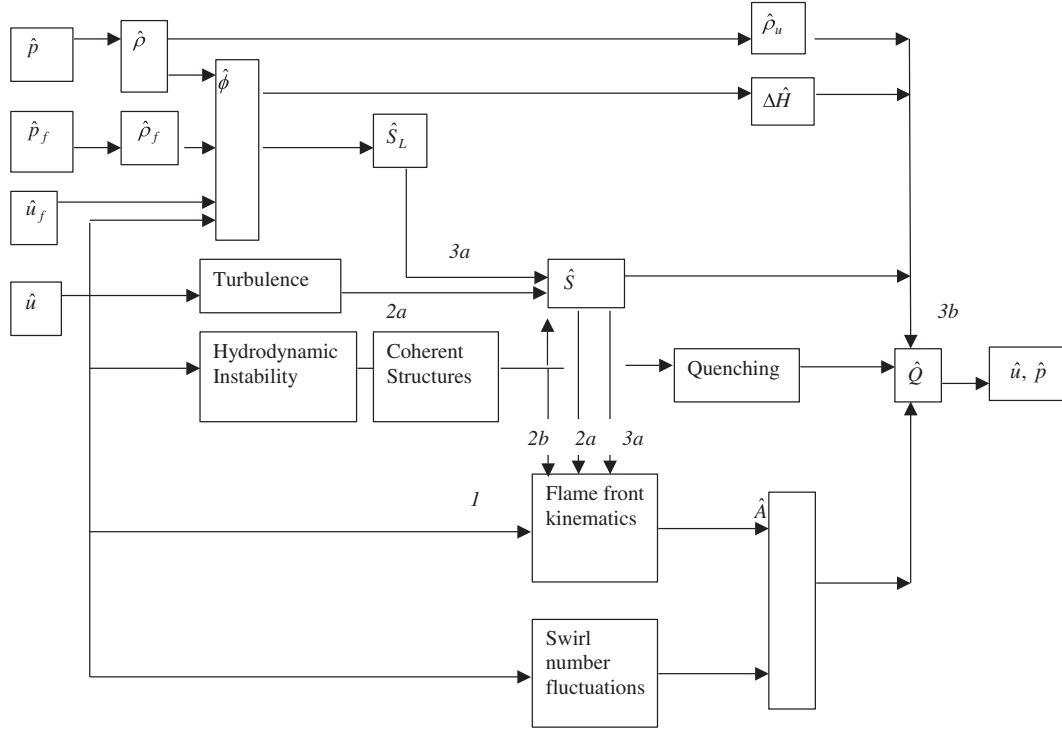


Figure 5. Overview of acoustic interactions in the flame from Lawn and Polifke,³⁹ reproduced with the permission of Taylor and Francis.

(1) Kinematic perturbations to the flame front area (wrinkling); (2a) Local shearing effects on burning velocity and flame area; (2b) Large scale vortex shedding effects on burning velocity and flame area; (3a) Equivalence ratio perturbations to the burning velocity and flame area; (3b) Equivalence ratio perturbations to the local heat release rate.

these can generate substantial perturbations in heat release, including even flame extinction.

3. *Acoustic pressures in the inlet of the burner resulting in fluctuations in the air or fuel supply, or both.* These generate equivalence ratio fluctuations, which perturb the burning velocity and hence the rate of heat release after a time lag due to convection from the point of mixing of air and fuel.

All of these mechanisms are associated with a time delay which is a function only of the flow-field. This is the reason for the close to linear increase in the phase of the FTF with increasing frequency that is seen in most configurations, e.g. in Hosseini et al.⁴¹ A method for separating the contributions experimentally has been proposed by Zellhuber et al.⁴²

It has recently been pointed out, independently by Hoeijmakers et al.⁴³ and by Emmert et al.,⁴⁴ that acoustic feedback from the flame surroundings is not necessary to generate instability. Intrinsic instabilities may arise because the outgoing acoustic wave moving upstream may influence the velocity perturbations in the flame, thus providing a mechanism for feedback and instability.

In such burners as the one discussed above, the flame interaction is through the acoustic velocities. However, in rockets, for example, the pressure fluctuations directly influence the combustion rate as well as the ones in velocity.⁷

2.3 Amplification in thermoacoustic engines

In the absence of a flame, thermal energy is not put directly into the gas but must be literally ‘transferred’ from adjacent surfaces. This is normally achieved with finely divided material through which the gas flows, making up a ‘regenerator’, if it is sufficiently closely coupled to the gas, or a ‘stack’. The crucial parameter is the time constant for heat transfer related to the thermal capacity of the gas. In terms of a heat transfer coefficient, h , the time constant characterising q in equation (1) is

$$\tau_h \equiv \frac{\bar{\rho} C_p A L}{A_s h} \quad (5)$$

where L is the length, A is the cross-sectional area of the gas passage and A_s is the heat transfer area, allowing that equation to be written for steady oscillations.

We now translate to the frequency domain for steady oscillations and make p_1 , u_1 , q_1 and T_{a1} the relevant complex amplitudes of the first harmonic at frequency ω , so that $P = \bar{P} + \text{real}(p_1 e^{j\omega t})$, etc.

$$\bar{\rho} C_p \left\{ j\omega T_{a1} + \frac{T_{a1}}{\tau_h} \right\} = j\omega p_1 - \bar{\rho} C_p \left\{ u_1 \frac{d\bar{T}}{dx} + \bar{U} \frac{dT_{a1}}{dx} \right\} \quad (6)$$

More rigorously than defining a heat transfer coefficient for unsteady conditions, the extent to which the gas follows the temperature of the adjacent surfaces can be characterised by a diffusion time constant (the time required for thermal diffusion across the characteristic dimension of the passages r_h) or by the non-dimensional ratio of r_h to the thermal penetration depth, $\delta_\kappa = \sqrt{\frac{2\kappa}{\omega}}$, where κ is the thermal diffusivity of the fluid. The ratio is known as the Lautrec number $La \equiv \sqrt{\frac{r_h^2 \omega}{2\kappa}}$ and thus the time constant is $\tau \equiv \frac{r_h^2}{2\kappa}$. Clearly, these parameters are related through the frequency so that

$$\omega\tau = La^2 \quad (7)$$

It is shown in Section 4.2 that this time constant is also proportional to τ_h defined in equation (5) for the asymptotic case of quasi-isothermal contact (regenerator-based engines). Tightly spaced surfaces of negligible thermal capacity are required for a regenerator, but there is a trade-off with increasing frictional and thermal dissipation as the hydraulic radius is reduced.

That is the reason why in regenerator-based thermoacoustic engines, the position of the regenerator must be chosen so that the acoustic impedance is high; otherwise, viscous dissipation (proportional to the square of velocity) overcomes acoustic power production.

The movement of thermal energy down a temperature gradient, in the case of a prime mover, or up, in the case of a refrigerator, can be described by reference to Figure 6(a) and (b), which are for a standing wave. Taking a Lagrangian view, as a particle moves to a hotter environment while gaining acoustic pressure in Figure 6(a), equation (1) indicates that it will warm up due to both the compression and the heat transfer from the adjacent surfaces. When the direction of motion reverses, cooling due to expansion takes place, eventually supplemented by heat losses to the surfaces. The Rayleigh criterion is satisfied because there is net heat addition at the time of greatest compression, and so energy is fed into the acoustic motion. On the other hand, in Figure 6(b), greatest compression is accompanied by heat loss to the surfaces, thermal energy is pumped up the temperature gradient, cooling the cold end, and external excitation, say by a loudspeaker, is required to sustain the acoustic oscillation. Alternatively, these processes may be viewed (as in equation (6)) as heating by compression, with a time delay related to the rate of heat transfer, modified by acoustic convection along the temperature gradient.

In travelling wave engines, on the other hand (Figure 6(c) and (d)), the objective for the regenerator

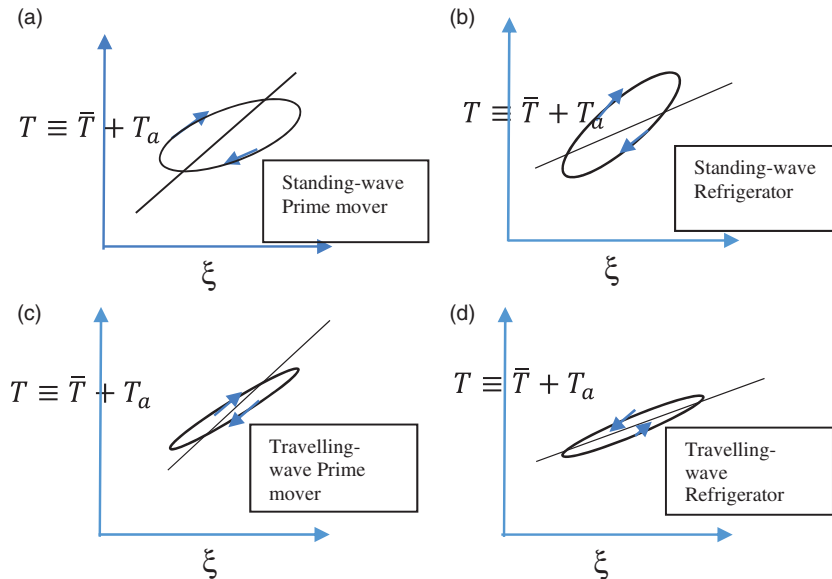


Figure 6. Temperature variation of the gas with acoustic displacement in a stack or regenerator, relative to the temperature gradient of the material. Standing-wave devices (a and b) involve a phase delay due to the thermal lag of the gas relative to the stack. Travelling-wave devices (c and d) have a gas in intimate contact with the regenerator.

is that its material should be so closely coupled to the gas thermally that, as the individual gas particles are displaced, they follow the temperature of the adjacent material closely, only deviating from it because of the compression and rarefaction. Maximum compression is associated with maximum velocity and no displacement, so this is where the maximum heat addition is required. The opposite effects are seen in the Stirling refrigerator cycle in Figure 6(d), where the acoustic energy is flowing in the opposite direction to that in Figure 6(c), down the temperature gradient.

In standing-wave devices, with the displacement and the pressure almost in-phase, it is desirable according to the Rayleigh criterion for there to be a phase-lag of close to 90° between the heat transfer and the acoustic velocity. Thus, performance is improved by adjusting the power absorption device in a prime mover, or the excitation device in a refrigerator, to adjust the lag in heat transfer relative to the acoustic velocity.

The temperature gradient in these devices is sustained by the heat transfer to external heat exchangers from the gas oscillating in and out at the two ends, where the temperature history becomes asymmetric. A high temperature heat source relative to ambient is required for a prime mover, while a refrigerator creates a cold reservoir if the high temperature end is anchored to ambient.

For an oscillation of frequency ω , a time constant τ_h which does not vary in time, and no mean velocity, equation (6) may be solved for steady oscillations to yield

$$\bar{\rho}C_p T_{a1} = \frac{j\omega\tau_h}{1 + j\omega\tau_h} p_1 - \bar{\rho}C_p \frac{d\bar{T}}{dx} \frac{\tau_h}{1 + j\omega\tau_h} u_1 \quad (8)$$

The enthalpy flow $H \equiv \text{real}\left\{\frac{A\bar{\rho}C_p u_1^* T_{a1}}{2}\right\}$ relative to the acoustic power $W \equiv \text{real}\left\{\frac{A p_1 u_1^*}{2}\right\}$ may now be evaluated at the hot and cold ends by multiplying equation (8) by u_1^* , with the asterisk denoting the conjugates of the complex amplitudes. For real fluids, cross-sectional averages of H and W must be taken (see Section 3.1). By conservation of total power

$$Q_h + W_h = Q_c + W_c \quad (9)$$

where Q_h and Q_c represent the rate of heat transfer from the gas in the hot heat exchanger and to the gas in the cold one. The efficiency of the stack

$$\eta \equiv \frac{W_h - W_c}{-Q_h} \quad (10)$$

may then be calculated for a travelling wave prime mover, a linear temperature distribution and a given

temperature ratio between hot and cold ends.⁴⁵ Some results for different lengths of regenerator (and hence different temperature gradients) are shown in Figure 7 as a function of $\omega\tau$ for a fixed frequency, thus illustrating the effect of the time constant. Clearly, a short time constant is required if efficiencies are to approach that of the Carnot cycle. (The efficiency is 0.42 for a temperature ratio of 3, for which the Carnot efficiency is 0.67.)

2.4 Comparison of feedback mechanisms and time delays

While equation (2) for the acoustic velocity gradient applies equally to stacks and to flames, the different nature of the thermal processes leads to somewhat different expressions for the acoustic temperatures. As has been seen, both processes involve a time delay, but in a flame, the heat release often depends on the acoustic velocity at an earlier moment upstream when the convection of gas to the flame front begins

$$q_1 = \bar{\rho}C_p \frac{\partial \bar{T}}{\partial x} u_1 \exp(-j\omega\tau) \quad (11)$$

giving

$$\frac{du_1}{dx} = -\frac{1}{\gamma P} (j\omega p_1) + \frac{1}{T} \frac{\partial \bar{T}}{\partial x} u_1 \exp(-j\omega\tau) \quad (12)$$

again for steady oscillations. In the stack, on the other hand, the heat added to the wave depends on the quality of the heat transfer, and thus on the acoustic temperature fluctuation, since in equation (6)

$$q_1 = -\frac{T_a}{\tau_h} \quad (13)$$

This leads to

$$\frac{du_1}{dx} = -\frac{(j\omega\tau_h + \gamma)}{(j\omega\tau_h + 1)} \frac{1}{\gamma P} (j\omega p_1) + \frac{1}{T} \frac{d\bar{T}}{dx} \frac{u_1}{(j\omega\tau_h + 1)} \quad (14)$$

It can be seen that there is very similar dependence on the pressure and on the temperature gradient for the small $\omega\tau_h$ of interest for regenerators. However, the introduction of a time constant τ_h to describe the thermoacoustic process is not usually appropriate for stack-based engines (as will be shown in Section 4.2), while $\omega\tau$ may be several radians in flames.

2.5 Heat release affecting frequencies

The effect of the heat released or transferred on the frequency of excitation is best illustrated with reference to the standing-wave with close to half a wavelength in

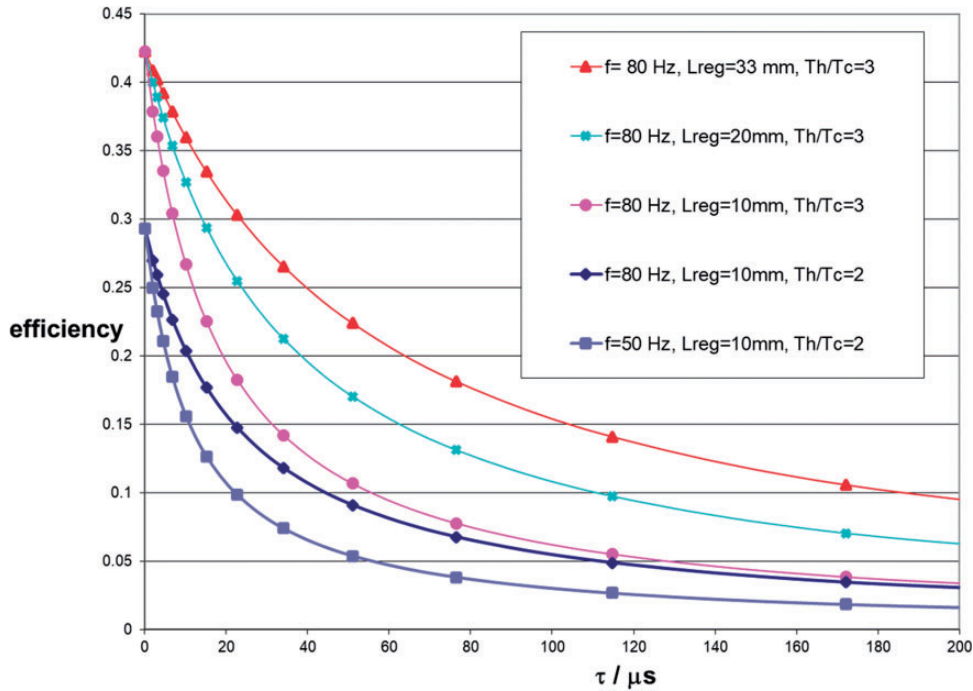


Figure 7. Efficiency of conversion of heat to acoustic energy in a travelling-wave thermoacoustic engine as a function of the time constant for thermal penetration in the regenerator, the regenerator length and the temperature ratio (from Lawn⁴⁵).

a Rijke tube (Figure 8). This is perturbed by the velocity jump so that the frequency is lower than would be calculated from the likely speed of sound at the tube exit where the gas provides the inertial mass and a wavelength twice the length of the tube (after end corrections). For instance, as illustrated qualitatively in Figure 8(a), for an actual tube ('furnace') length of 1000 mm, corrected to 1.08 m, even a temperature of only 400 K would suggest a frequency of not less than 185 Hz, as opposed to the 175 Hz that was observed (Figure 9, taken from Lawn³⁷). A vector diagram of the velocities further illustrates the role of the phase change at the flame (Figure 8(b)). Because there is some energy loss by radiation at the two open ends of the tube, the velocity vectors must have opposite real components to satisfy the extended Rayleigh criterion.

Since the time delay giving rise to the change in phase of the velocity at the flame is affected by any change in the combustion conditions, an increase in the airflow rate, blowing a flame further from the burner and increasing the time delay before the velocity for stabilisation can be reached, can lead to a reduction in the frequency. Moreover, for any given length of tube, there is only a range of air flows for which the time delay is able to give rise to the required phase change, and excitation to occur (Figure 9). Note that changing the burner 'tip', and hence the configuration

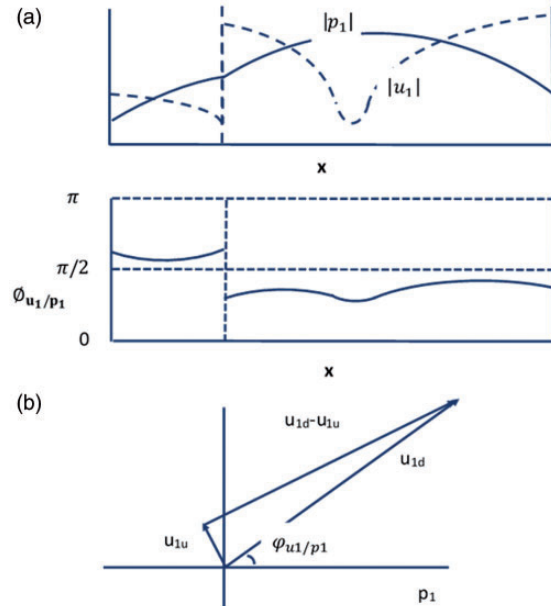


Figure 8. (a) The fundamental mode in a Rijke tube, with heat input at the dotted line. In this instance, the resulting velocity jump, increasing the gradient of the pressure, ensures a lower frequency than with no heat input. (b) The phase diagram for the velocity amplitudes at this frequency on the two sides of the heat input, which is related to $u_{1d} - u_{1u}$ through equation (3).

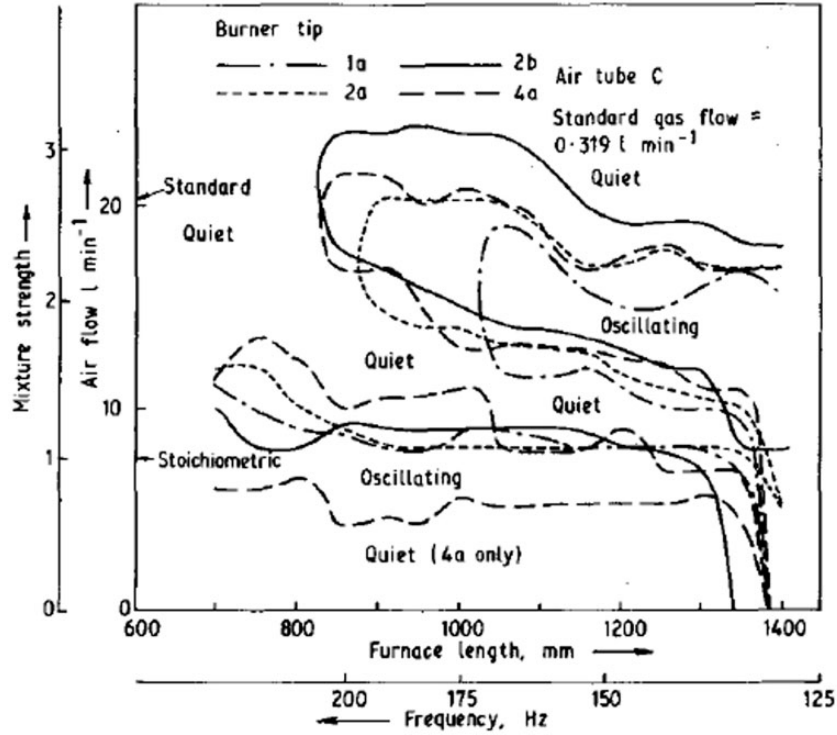


Figure 9. The effect of the air supplied to a diffusion flame in Rijke tubes ('furnaces') of various lengths on the propensity for excitation. The zones of excitation are affected by the burner tip, but the frequency only depends significantly on the length of the tube (from Lawn³⁷).

of the flame, also has an effect on the airflow range for excitation.

Factors affecting chemical reaction rates, such as the precise composition of the fuel and the equivalence ratio, can also have a significant effect on the overall combustion delay time, and hence on the frequency of excitation, for instance in a pulse combustor.⁴⁶

3. Modelling and measurement of linear acoustics

3.1 One-dimensional modelling and measurement in engines and combustion systems

Most attempts to analyse even complex thermoacoustic systems have computed the transfer of plane acoustic waves in ducts that are taken to be one-dimensional. In the case of thermoacoustic engines, in which the interaction of surfaces with the acoustic waves is crucial, the effects of the boundary layers have been built into the equations by the use of 'Rott functions', f_v and f_k .^{24,47} Linear thermoacoustic theory is mostly based on the two approximations that the amplitudes of acoustic oscillations are small (linear acoustics) and that transverse gradients are much larger than axial gradients (boundary layer approximation). Rott functions involve the integration of solutions to the continuity,

momentum and enthalpy equations across the width of passages. Thus, the acoustics are described by

$$\frac{\partial p_1}{\partial x} = -\frac{j\omega\bar{\rho}\langle u_1 \rangle}{1-f_v} \quad (15)$$

and

$$\frac{\partial \langle u_1 \rangle}{\partial x} = -\frac{j\omega[1+(\gamma-1)f_k]}{\gamma\bar{P}} p_1 + \frac{f_k-f_v}{(1-\sigma)(1-f_v)} \frac{1}{\bar{T}} \frac{\partial \bar{T}}{\partial x} \langle u_1 \rangle \quad (16)$$

with the related equation for temperature fluctuations

$$\bar{\rho}C_p \langle T_{a1} \rangle = (1-f_k)p_1 - \bar{\rho}C_p \frac{1}{j\omega\bar{T}} \frac{\partial \bar{T}}{\partial x} \frac{(1-f_k)-\sigma(1-f_v)}{(1-f_v)(1-\sigma)} \langle u_1 \rangle \quad (17)$$

where $\langle u_1 \rangle$ and $\langle T_{a1} \rangle$ are now the acoustic amplitudes spatially averaged in the transverse direction, p_1 having been assumed uniform, and σ is the Prandtl number.

In segments where there is heat transfer, equation (16) is another representation of spatially averaged equation (14), and equation (17) of spatially averaged equation (8), and their equivalence allows the time

constant to be identified in terms of the Rott functions. Note that in the absence of a temperature gradient, the standard wave equation is recovered if the Rott functions are put equal to zero, but that the Rott equations are no longer valid to describe entrance effects (and therefore heat exchange) next to the stack terminations.

In the much used thermoacoustic calculation procedure for engines, the ‘Design Environment for Low-Amplitude Thermoacoustic Energy Conversion’, DeltaEC,⁴⁸ these equations are solved for a sequence of segments, handing on the primary variables, p and u from one segment to the next. The calculation uses a ‘shooting method’ to iterate on all variables simultaneously if the boundary conditions of the problem are remote from the first segment.

A similar approach is used by Lawn⁴⁹ when solving in a MATLAB program, except that a sequence of iteration procedures is used to converge to the boundary conditions one at a time, with later adjustment, when a later calculation disturbs an earlier fit. Thus, the conditions at the cold end of the regenerator are met first, and then those at the hot end, with some adjustment at the cold end then becoming necessary. If the configuration involves a loop, further iteration of the starting acoustic impedance is necessary to ensure a cyclic solution. A comparable procedure has been developed by Babaei and Siddiqui⁵⁰ for standing-wave refrigeration.

These calculation procedures are probably of little relevance to flame-driven systems, where

- (a) there is a straight-through flow and usually no loop;
- (b) even in closed-loop pressurised systems, the boundary conditions for the thermoacoustic calculation are supplied by compressors or turbines;
- (c) in straight-through systems, the boundary conditions can be applied directly to the flame element;
- (d) the relevant geometry is highly three-dimensional (see Section 3.2).

An alternative and more elegant approach, now used for both flames and engines, is to develop transfer matrices between ‘upstream’ and ‘downstream’ for each of the components of the burner and combustion chamber, or the segments of the engine.⁵¹

$$\begin{pmatrix} \frac{p_l}{\rho c} \\ \langle u_l \rangle \end{pmatrix}_d = \begin{pmatrix} T_{11} & T_{12} \\ T_{21} & T_{22} \end{pmatrix} \begin{pmatrix} \frac{p_l}{\rho c} \\ \langle u_l \rangle \end{pmatrix}_u \quad (18)$$

The transfer coefficients derived from equations (15) and (16) are modified where necessary to include heat transfer. The equations can then be solved simultaneously with the boundary conditions by matrix inversion.

Introducing characteristic acoustic amplitudes, representing waves travelling in opposite directions as

$$f \equiv \frac{1}{2} \left(\frac{p_l}{\rho c} + \langle u_l \rangle \right); \quad g \equiv \frac{1}{2} \left(\frac{p_l}{\rho c} - \langle u_l \rangle \right) \quad (19)$$

the transfer matrix may be transformed into a scattering matrix

$$\begin{pmatrix} g_u \\ f_d \end{pmatrix} = \begin{pmatrix} r_u & t_d \\ t_u & r_d \end{pmatrix} \begin{pmatrix} g_d \\ f_u \end{pmatrix} \quad (20)$$

where the coefficients can be evaluated from combinations of the T_{mn} transfer matrix components.⁵² As the name implies, the scattering matrix evaluates the waves emanating from the segment from a description of the waves incident upon it.

The crucial and difficult part of the calculation of the behaviour of a flame or a stack in a loop is the characterisation of the transfer matrix of that element. In both cases, there are models for the phenomena that can be translated to transfer functions (see Section 4). However, it is often desirable to actually measure the transfer function. Bannwart et al.⁵³ describe how this can be achieved for a regenerator by measuring the impedance at inlet and outlet (usually by the two-microphone method) in two separate experiments with sources on different sides. The transfer function can then be applied in configurations with completely different boundary conditions.

A similar technique is used extensively for flames, for which the data for naturally occurring flame oscillations are often supplemented by introducing a siren or loudspeaker before the fuel mixture plenum. In the particular study by Schuermans et al.,⁵⁴ the transfer function data are fitted to a simple model of the flame excitation process. However, a more usual procedure in view of the difficulty of acoustic measurements in the hot combustion gases is to excite the incoming flow and then to measure the heat release response ‘directly’ by recording the UV chemiluminescent emissions. Palies et al.⁵⁵ analyse such data in terms of an ‘effective’ damping, the difference between the actual damping and the growth rate induced by the flame, which is determined from the half-width of the frequency response. This allows the actual damping to be deduced from low amplitude excitation. This and three other techniques (impulse response for linearly stable systems, stabilisation by active control, and white noise excitation) are explored by Mejia et al.⁵⁶ for a laminar flame.

The acoustic impedance of fuel and air supply lines has been measured by a reflection technique on the

assumption that there are devices in the line that decouple the downstream sections from the upstream.⁵⁷ The impedances of these devices (in this case, flow controllers) are determined offline and then combustion noise is used to generate the signals that are reflected from them in situ.

These experimental techniques could be applied to engines. In a theoretical treatment using a Green's function that could also be applied to engines, Kosztin et al.⁵⁸ show that the temperature jump across a flame can be modelled (with measured boundary inlet and outlet conditions) so as to predict the measured fundamental eigenmode of acoustic pressure quite accurately. The details of the temperature field are not necessary: uniform upstream and downstream temperatures can be assumed.

3.2 Modelling of annular combustors and devices with centred regenerators

A particular configuration of interest in the thermoacoustics of flames is the annular supply chamber and combustor, connected through a large number of burners, that is adopted in most industrial gas turbine designs. Instead of individual combustion cans for a ring of burners around the main axle of the turbine, the combustion zones of these burners all communicate freely around an annulus. Because of the prevalence of azimuthal acoustic modes, this clearly cannot be treated one-dimensionally. It has been shown, however,⁵⁹ that sometimes it is the axial flame response that is important, as in single burner tests, and then it is possible to construct models in which the azimuthal modes in the plenum and combustion chambers are computed analytically, with one-dimensional linkage through the burners and flames.⁶⁰ In a variant of this approach to calculate the eigenmodes, the Helmholtz equation is solved rigorously by finite element methods in the supply and combustion chambers.⁶¹ This type of coupling method has been confirmed with full LES simulation of the chambers.⁶²

In thermoacoustic refrigeration, the desire for compact devices has also led to annular designs, such as that explored by Poignand et al.⁶³ or the thermoacoustic chiller developed at Penn State University.⁶⁴ However, these authors rely on lumped parameter modelling of their two cavities (compressible gas volumes) which are small compared with the wavelength, coupled by one-dimensional wave propagation in the regenerator and in the annular return passage. Others have published full numerical simulations for the annular return geometry,⁶⁵ but none of these approaches is obviously applicable to combustion chambers.

4. Modelling of thermoacoustics with heat addition

4.1 Heat release in flames

The mechanisms of thermoacoustic instability described in Section 2.2 can be expressed as linear perturbations of the heat release equation for a flame

$$Q = \rho_u A S \Delta H \quad (21)$$

where ρ_u is the instantaneous upstream mixture density, S is the turbulent burning velocity, A is the flame area, and ΔH is the enthalpy of combustion. To first order, i.e. for small perturbations

$$\frac{q}{Q} = \frac{\rho_{au}}{\rho_u} + \frac{a}{A} + \frac{s}{S} + \frac{\Delta H_a}{\Delta H} \quad (22)$$

Except at high Mach number, the perturbations in upstream density ρ_{au} are generally negligible, and in the absence of equivalence ratio perturbations, so too are those in enthalpy ΔH_a . The perturbations in area may be due to more than one mechanism.

However, as already noted, nearly all processes involve some form of time delay. Crocco⁶⁶ recognised this for rocket propulsion in proposing the so-called ' n - τ model', in which the index n is the ratio of amplitudes in the generic response equation

$$\frac{q_1}{u_1} \equiv n e^{-j\omega\tau} \quad (23)$$

and n can either be identified through detailed evaluation of equation (22) or as

$$n \equiv \left| \frac{q_1}{u_1} \right| = \frac{\bar{Q}}{\bar{U}} = \bar{\rho} C_p \frac{\partial \bar{T}}{\partial x} \quad (24)$$

as already assumed in equation (11). With this model for the heat release, equation (3) for the velocity jump across a concentrated flame becomes

$$u_{d1} - u_{u1} = \int u_1 e^{-j\omega\tau} \frac{1}{\bar{T}} \frac{\partial \bar{T}}{\partial x} dx \quad (25)$$

More descriptive models can be constructed, for example for laminar conical flames,^{32,67} for V-flames^{8,68} and for swirl burners.⁶⁹ These all rely on some empiricism and assumptions about the flame structure if the flow is turbulent, but they incorporate timescales reflecting the convection of fluid or vortices from the point at which the incident acoustic perturbation is defined to some part of the flame front. Thus, the frequencies generated vary monotonically with \bar{U} and the time delay of the local heat release can be

correlated by $\omega\tau = 2\pi f(x - x_0)/\bar{U}$, where x_0 is an effective origin for the acoustic wave. An example of the predicted variation of the FTF with frequency is shown in Figure 10. If the flame is laminar and the flow-field deliberately simple, very accurate representations of its wrinkling behaviour can be produced.⁷⁰

These examples are all for premixed flames. In the diffusion flames of a pulse combustor, times associated with mixing rates and with chemical kinetic rates are dominant.⁴⁶

These models assume that the flame is ‘compact’: that is the axial extent of heat release is much shorter than the wavelength. The effect of ‘non-compactness’ has been explored by Leandro and Polifke.⁷¹ Increasingly, though, LES is being used to compute the FTF, with the advantage that the compactness assumption can be abandoned and the non-linear interactions generated by extreme wrinkling can also be examined.

4.2 Heat transfer in regenerators and stacks

The basis for computing the performance of engines and refrigerators has already been laid out in Section 2.3, since the Rott equations can be applied to each of the elements that comprise the complete engine, from the thermoacoustic core itself to the acoustical network to which it is connected. The stack/regenerator and the heat exchangers are treated by means of a capillary-tube based theory, or in other words as a stack of straight channels submitted to a temperature gradient. Swift²⁵ gives expressions for the Rott parameters, f_v and f_κ , in various geometries of straight-through channel. Arnott et al.⁷² introduced a function from porous media theory which is essentially $1-f_\kappa$ and evaluated it for various cross-sections of channel, so the approach to generating one-dimensional equations is the same. However, many engines make use of stack/regenerator materials with complex geometries such as a pile of stainless steel meshes or carbon foams, so that using Rott’s theory is questionable. The experiments performed by Wilen⁷³ show that a tortuous material like a Reticulated Vitreous Carbon Foam can be reasonably described by means of the Rott parameters. For such tortuous passages, including those formed by layers of woven mesh, Swift and Ward⁷⁴ advocate the use of friction factors derived from steady flow experiments. Lawn⁷⁵ showed experimentally for a coarse and a fine mesh that the steady friction factors are valid to within 20%, at least for Lautrec numbers below 0.6.

In this limit of diameters of channel very much smaller than the penetration depth, the Rott parameters all tend to a very similar limit (no matter the geometry) when y_0 is identified as the hydraulic radius, the ratio of the flow area to the perimeter of the passage, which is

half the actual radius for circular pores. For parallel plates, this limit is given by

$$1 - f_\kappa \rightarrow j\omega\tau_h \rightarrow \frac{2jy_0^2}{3\delta_\kappa^2} \quad (26)$$

Thus, we can identify

$$\tau_h = \frac{\sigma y_0^2}{3\nu} = \frac{y_0^2}{3\kappa} \quad (27)$$

for a regenerator.⁴⁵ In the absence of mean flow (not always the case, see Section 4.5), the time constant for engines with fixed geometry is thus inversely proportional to the thermal diffusivity. As explored in the Section 4.3, this only varies with the mean temperature.

In the limit of diameters of channel much larger than the penetration depth, relating f_κ to the time constant τ_h is not possible. However, by applying the large pore approximations to Rott’s theory leads, in the time domain, to the following expression for the rate of heat released to the fluid per unit volume (derived on the basis of the theory of Sugimoto⁷⁶)

$$q = \frac{\bar{\rho}C_p\bar{T}}{y_0} \times \sqrt{\nu} \left[\frac{\gamma - 1}{\sqrt{\sigma}} \frac{\partial^{-1/2}}{\partial t^{-1/2}} \left(\frac{\partial u}{\partial x} \right) + \frac{1}{\sigma + \sqrt{\sigma}} \frac{1}{\bar{T}} \frac{d\bar{T}}{dx} \frac{\partial^{-1/2} u}{\partial t^{-1/2}} \right] \quad (28)$$

where the fractional derivative operator is defined as

$$\frac{\partial^{-1/2} f}{\partial t^{-1/2}} = \frac{1}{\sqrt{\pi}} \int_{-\infty}^t \left(\frac{f(x, \theta)}{\sqrt{t - \theta}} \right) d\theta$$

and has the physical meaning of a memory effect. (The second term on the right hand-side, proportional to the temperature gradient, therefore acts as a feedback driving self-sustained thermoacoustic oscillations.) Should the gas be considered as inviscid ($\nu = 0$) and should the oscillations be purely harmonic at angular frequency ω (so that the fractional derivative reduces to a delay function), equation (28) reduces to

$$q_1 = \frac{\bar{\rho}C_p\bar{T}}{y_0} \sqrt{\kappa} \frac{1}{\bar{T}} \frac{d\bar{T}}{dx} \frac{1}{\sqrt{\omega}} u_1 \left(t - \frac{\pi}{4\omega} \right) \quad (29)$$

which is very similar to equations (11) or (23) for a flame, although there the time delay is related to the burner load, through $\tau = (x - x_0)/\bar{U}$.

In practice, thermoacoustics with flames are often described by means of the rate of unsteady heat release, q , but this is rarely the case for stack/regenerator based

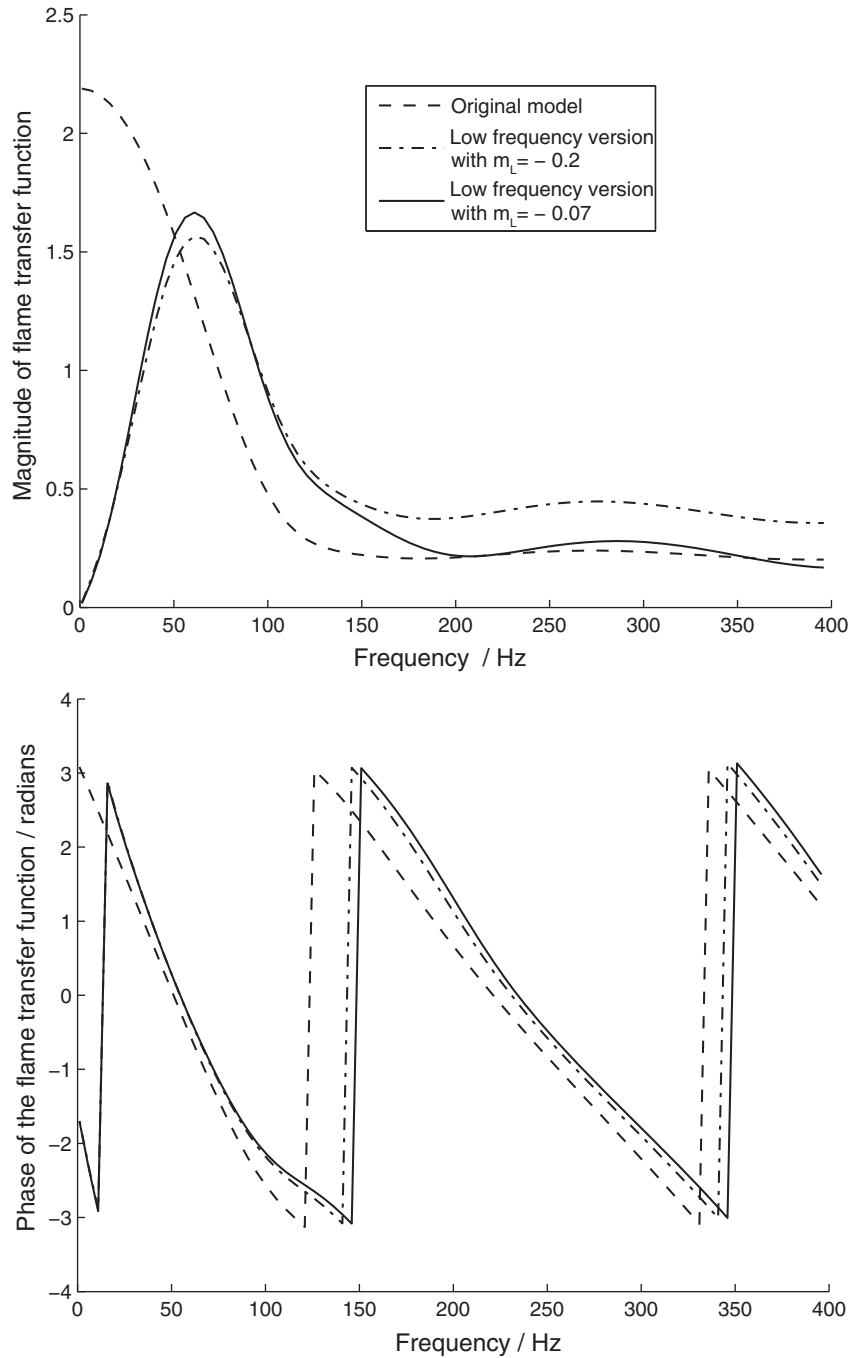


Figure 10. Predicted transfer function for a model gas burner for the processes shown schematically in Figure 5, from Polifke and Lawn.⁶⁹ The original flame model³⁹ is shown in Polifke and Lawn⁶⁹ to have not properly conserved mass flow through the flame.

engines, for which an energetic balance in the frequency domain is usually preferred to predict the amplitudes of a limit cycle. If the temperature distribution in the stack/regenerator and in the thermal buffer tube is known, and once the acoustic field is calculated (which can be done by treating each element as a two-port with equations (15) and (16)), the acoustic

power added or subtracted by the stack is given by⁷⁷

$$\frac{dW}{dx} = A \frac{dp_1 u_1^*}{dx} \quad (30)$$

where A is the cross-sectional area of the gas passages in the stack/regenerator. The prediction of a

steady-state regime is then realised from the conservation of enthalpy flow, where the time-averaged acoustically induced heat flux (or thermoacoustic streaming) can also be evaluated from Rott's theory (for more details, see Swift⁷⁷ or Tominaga⁷⁸). Equation (30) is adequate for most purposes, but a number of investigators are now using CFD to examine the thermoacoustic characteristics of stacks without any explicit boundary layer approximation.⁷⁹

Again in the limit of diameters of channels much larger than the penetration depth, and for a short stack (Δx in length) subjected to a standing-wave in an inviscid gas, Swift⁷⁷ has shown that

$$W = \frac{1}{4} \Pi \Delta x \delta_\kappa \frac{\omega}{\bar{T}} \frac{1}{\bar{\rho} C_p} \left\{ \frac{\frac{\partial \bar{T}}{\partial x}}{\left(\frac{\partial \bar{T}}{\partial x} \right)_{crit}} - 1 \right\} p_1^2 \quad (31)$$

where Π is the lateral dimension of the heat transfer surface and where the critical temperature gradient, the one above which thermoacoustic amplification, occurs

$$\left(\frac{\partial \bar{T}}{\partial x} \right)_{crit} = j \frac{\omega}{\bar{\rho} C_p} \frac{p_1}{u_1} \quad (32)$$

corresponds to the ratio of the peak amplitude of temperature oscillations ($p_1/\bar{\rho} C_p$) to the acoustic displacement amplitude ($u_1/j\omega$).

It is instructive to return to the case of short regenerators in the limit of a low Lautrec number (i.e. channels much smaller than the penetration depth) with an inviscid gas. By applying a forward Euler finite-difference scheme to equation (14) for the case of very narrow pores, the power production can be represented by a velocity jump (see Swift²⁵ for more details)

$$u_{d1} - u_{u1} = u_{u1} \frac{(\bar{T}_d - \bar{T}_u)}{\bar{T}_u} \quad (33)$$

which is consistent with equation (25) for flames, since $\frac{u_1}{T} = \frac{u_{1u}}{T_u}$ by continuity in a compact flame, and there is no time delay.

4.3 Effects of gas composition, temperature and pressure

For the thermoacoustic engine, Olsen and Swift⁸⁰ have carried out a full non-dimensional analysis, showing that for a fixed regenerator geometry, the frequency of a prime mover scales as $\frac{c_{ref}}{L}$ and is a function of γ , σ , La and $\frac{Q}{\bar{P} A c_{ref}}$. Moreover, the acoustic temperature, pressure and velocity are also functions of these dimensionless groups and scale as \bar{T}_{ref} , \bar{P} , c_{ref} , respectively. Finally, the acoustic power scales as $P A c_{ref}$ and is a

function of the same dimensionless parameters. Through the time constant identified in Section 2.3, we see that the crucial parameter is $La \propto \frac{1}{\sqrt{\kappa}}$, although γ and σ also have an independent role. The Prandtl number should be as low as possible, which can be realised using a mixture of monoatomic gases, typically a mixture of helium with a heavy gas, either xenon or argon (see Tijani et al.⁸¹ for more details). The specific heat ratio γ impacts the sound speed $c_{ref} = \sqrt{\gamma R \bar{T}_{ref}}$ and it is also directly involved in power production since we can see from equation (31) that $W \propto (\bar{T}_{ref} \bar{\rho}_{ref} C_p)^{-1} \propto \frac{\gamma-1}{\gamma}$. The values of these parameters for some common gases at two pressures are shown for $\bar{T}_{ref} = 600$ K in Table 1. Thus, a light monoatomic gas at high pressure will have an advantage in having high thermal diffusivity and allowing high efficiency. The high speed of sound allows a more compact loop, but while the high pressure confers high energy density and high amplitude, it also requires smaller pores in the regenerator.

Raspet et al.⁸² develop a theory to account for the much-reduced onset temperature in inert gas systems when a condensing vapour is introduced. They show that vapour diffusion in the pores of the stack is added to the normal heat diffusion effect. The surprising performance of the Kibitsunokama described in the Introduction is thus partially explained. Also, making use of a mixture of inert gas and condensing vapour as a working fluid is a promising way of decreasing the required temperature gradient along the stack.

For flames on the other hand, there is less flexibility in the choice of the working medium, because of the need for oxygen and the once-through nature of the system. Diluents other than nitrogen may be possible but the effect on the flame will be variable so that generalisations about the structure of the flame are not possible. The first-order effect of pressure will be to shorten the flame and reduce the relevant time delays, so that higher frequencies will be excited in a fixed geometry.

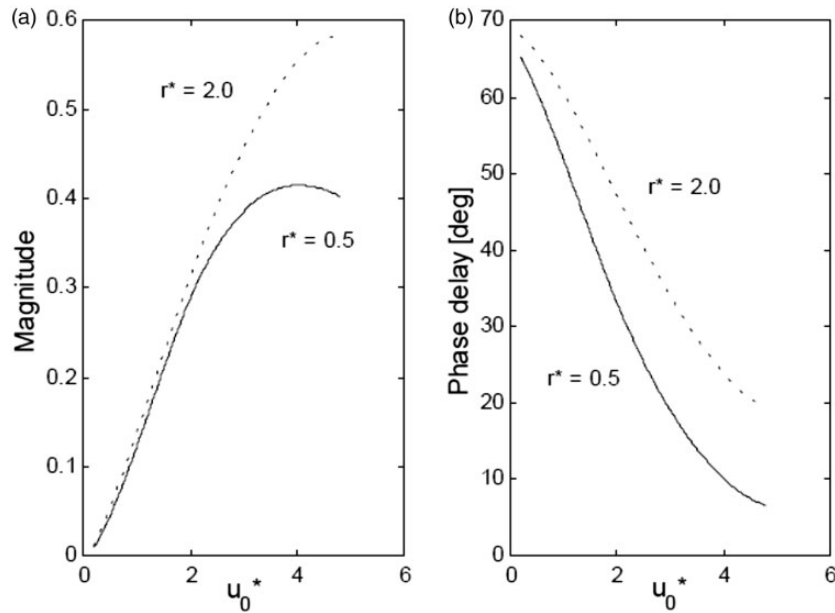
4.4 Rijke tubes

With the background of the modelling summarised in sections 4.1 and 4.2, we return to the geometry in which flames and engines can be most readily compared. Specific modelling and experiments on the Rijke tube have been comprehensively reviewed by Raun et al.⁸³

In a Rijke tube driven by a heated gauze (Figure 1(b)), there is usually a mean buoyancy flow through the gauze. (In some experiments, the tube is horizontal and a mean flow is imposed either by blowing or sucking, thus affording greater control.) It is necessary to describe the heat

Table I. Properties of the common thermoacoustic gases.

Gas	P /bar	T /K	ρ /(kg/m ³)	c /(m/s)	ρc /(kg/m ² /s)	κ $\times 10^5$ /(m ² /s)	δ_κ	δ_κ /mm	δ_κ
f/Hz							50	80	200
Air	1	300	1.18	347	408	2.2	0.37	0.30	0.19
	1	1000	0.35	634	224	17	1.03	0.81	0.51
	30	300	35.3	347	12300	0.07	0.07	0.05	0.03
	30	1000	10.6	634	6710	0.56	0.19	0.15	0.09
Ar	1	300	1.62	323	524	2.1	0.37	0.29	0.18
	1	1000	0.49	590	287	17	1.03	0.82	0.52
	30	300	48.7	323	15700	0.07	0.07	0.05	0.03
	30	1000	14.6	590	8620	0.56	0.19	0.15	0.09
He	1	300	0.163	1019	166	18	1.06	0.84	0.53
	1	1000	0.049	1860	91	140	3.02	2.39	1.51
	30	300	4.89	1019	4980	0.59	0.19	0.15	0.10
	30	1000	1.46	1860	2720	4.8	0.55	0.44	0.28

**Figure 11.** Amplitude and phase of the transfer function from a wire with varying mean flow velocity, where $U_0^* \equiv \frac{\bar{U}}{\sqrt{\kappa\omega}}$, as a function of the radius, where $r^* \equiv r\sqrt{\frac{\omega}{\kappa}}$, based on the results of Kwon and Lee⁸⁵ with $u/\sqrt{\kappa\omega} = 1$ (from Matveev⁸⁴).

transfer from the gauze to the oscillating flow. Matveev⁸⁴ uses the computational results from Kwon and Lee⁸⁵ for a single cylinder in fluctuating cross-flow. These are reproduced in Figure 11. A linearised correlation for one case can be written

$$\frac{q_1}{\bar{Q}} = 0.15 \frac{u_1}{\bar{U}} \left(\frac{\bar{U}}{\sqrt{\kappa\omega}} \right) \exp \left\{ -j \left(70 - 11 \frac{\bar{U}}{\sqrt{\kappa\omega}} \right) \frac{\pi}{180} \right\} \quad (34)$$

for $\frac{\bar{U}}{\sqrt{\kappa\omega}} < 4$ and $r\sqrt{\frac{\omega}{\kappa}} = 2$, where r is the cylinder radius. The interesting feature of this formulation is that the

phase delay diminishes from about 70° as the velocity increases. With careful modelling of the heat exchange in the rest of the Rijke tube, Matveev⁸⁴ achieved good agreement with experiment for the dependence of the mean flow at the stability boundary on the heater power (Figure 12).

However, it is well known that cylinders in cross-flow actually exhibit the King's law dependence

$$Q \propto U^{0.5} \quad (35)$$

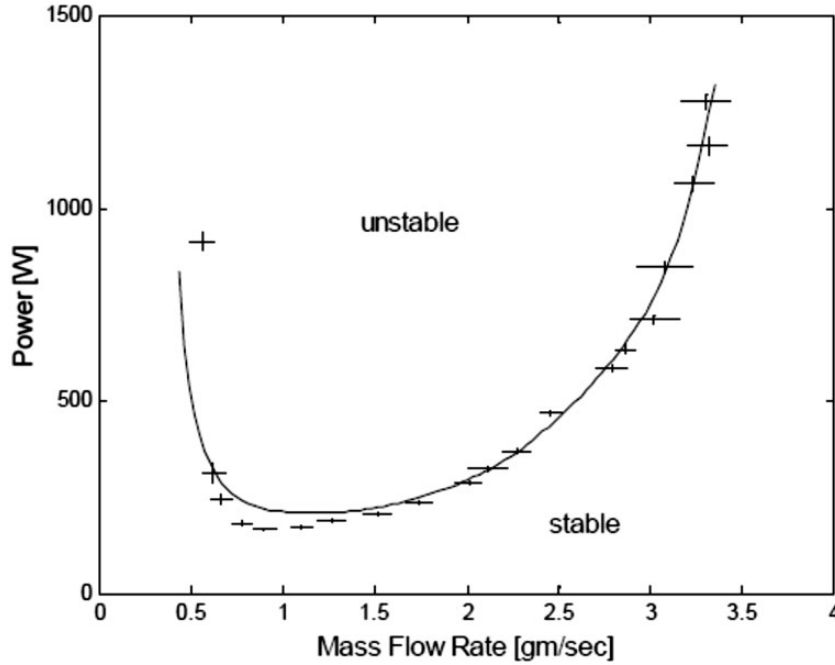


Figure 12. Comparison of the experimental (crosses) and calculated (solid line) results for the power to the heat source at one quarter of the length that gave rise to transition to instability in a Rijke tube. The calculations used a linearised transfer function from Figure 11 (from Matveev⁸⁴).

as was confirmed for a heated grid by Torszynski and O'Hern,⁸⁶ and that this leads to

$$\frac{q}{Q} = 0.5 \frac{u}{U} \quad (36)$$

to first order. For a pure standing-wave, this would yield zero energy input because it takes no account of the inherent time delay due to thermal diffusion. Heckl⁸⁷ took this into account with a non-linear expression (due to Lighthill) that incorporated a time delay given by

$$\tau_h = \frac{2r}{U} \quad (37)$$

which obviously diminishes with increasing velocity. She then showed that her expression allowed the experimentally determined limit cycles to be accurately modelled. In a later chapter of his thesis, that was quoted above, Matveev⁸⁴ took a somewhat different approach, assuming that the non-linear transfer function was the product of the dependence on frequency discussed earlier and a non-linear term which was the same as that given by a quasi-steady perturbation of equation (35). The time delay given by Kwon and Lee⁸⁵ was thus retained, so even the non-linear modelling included a similar tendency for the time delay to be inversely proportional to the mean velocity, as has already been described for flames.

If the flames in a Rijke tube are sufficiently thin, the time delay τ may be comparable to τ_h for a red-hot gauze. Thus, the change in acoustic velocity will be similar to that across a gauze. In that case, similar frequencies of excitation in the same length of tube may be expected and the degree of similarity of these two different thermoacoustic phenomena most closely revealed. However, no direct experimental comparison of a flame and a heated gauze appears to have been published.

4.5 Non-linear mechanisms in thermoacoustics

The topic of non-linearity in both engine and flame systems has been introduced in Section 4.4 in the context of the Rijke tube. There are in fact many similarities between the departures from simple linear behaviour in the two systems, and hence there is scope for methods of analysing these to be applied to both. In his book, Swift²⁵ mainly treats linear behaviour in engines, but he does devote a whole chapter to the effects leading to non-linearities. The generic processes will now be considered.

There are essentially four processes that give rise to non-linearity in thermoacoustic systems. These are:

- (a) Fluid dynamic pressure losses due to high intensity acoustic perturbations that are not purely viscous and depend on something close to the second power of the acoustic velocity.

These arise in stack material, for which many investigators have shown a departure from the laminar proportionality of drag to velocity due to the wakes of mesh elements or stack plates. In channelled regenerators, the passages are normally too narrow for transition to turbulence to be an issue. (With a diameter of 0.5 mm and $\bar{U} = 5$ m/s, the Reynolds number at high temperature is still only about 50.) However, in more tortuous material, such as stacked woven screens, empirical data for pressure losses indicate that linear relationships hold quite well, as discussed in Section 4.2.

Outside the core, the so-called ‘minor losses’ in thermoacoustic loops, those occasioned by the transition to turbulence in bends or in sudden changes in pipe cross-section, such as orifices, are not necessarily minor in the context of the total dissipation. It is often convenient to treat them as step changes in the parameters of the acoustic path. Swift²⁵ discusses a number of configurations with loss coefficients based on steady-flow data. There is an extensive literature on acoustic flow through orifices, much of it generated for silencers and gas turbine liners, where minimisation of the reflected wave is the objective. Lawn⁸⁸ reviews this literature and proposes criteria for taking a simultaneous mean flow into account in computing the pressure losses, when the dissipation remains linear in $|u|^2$. Data on acoustic losses in bends are sparse but Olson and Swift⁸⁹ examined losses in U-bends, and Hossain et al.⁹⁰ investigated a number of bends with different radii of curvature.

(b) The coupling of acoustic parameters in the second-order terms of the equations, such as $\rho_a T_a$ in the energy equation (6) and $\rho_a u$ in the continuity equation, where ρ_a is the acoustic fluctuation in density.

The theory derived by Rott⁴⁷ to describe thermoacoustic engines is a linear theory leading to the calculation of time-averaged second order terms, namely the power $W = A\bar{p}\bar{u}$ and the thermoacoustic streaming $A(\bar{\rho}C_p\bar{u}T_a - \bar{p}u)$, where A is the cross-sectional area of the gas passage. When the power production is positive out of the stack at the hot end, the latter describes acoustically induced heat transfer from the hot to the cold source. This limits the temperature gradient in the stack (See (d) below.) Therefore, linear theories already include a saturation process leading to limit cycling, in so far as the equations describing wave propagation and sound amplification are coupled to the ones describing heat transfer through the thermoacoustic core.

However, there exist other time-averaged second-order terms which may impact heat transfer processes through the thermoacoustic core and which give rise to mean flow streaming. The main types of streaming are illustrated in Figure 13. In looped engines, the most important is the mean circulation (Gedeon streaming) driven from the cold to hot ends of the stack and thus reducing the achievable temperature gradient. The time-averaged mass flow due to the generation of acoustic streaming can be calculated numerically or using successive approximation methods (see Boluriaan and Morris⁹¹ for a review on this topic), but only for some configurations much simpler than the ones encountered in thermoacoustic engines. Research devoted either to the measurement or to the numerical calculation of the different types of acoustic streaming has been very active during the past 10 years.

In general, efforts are made in thermoacoustic engines to suppress any such mean flow, because heat is convected away from the hot heat exchanger into the

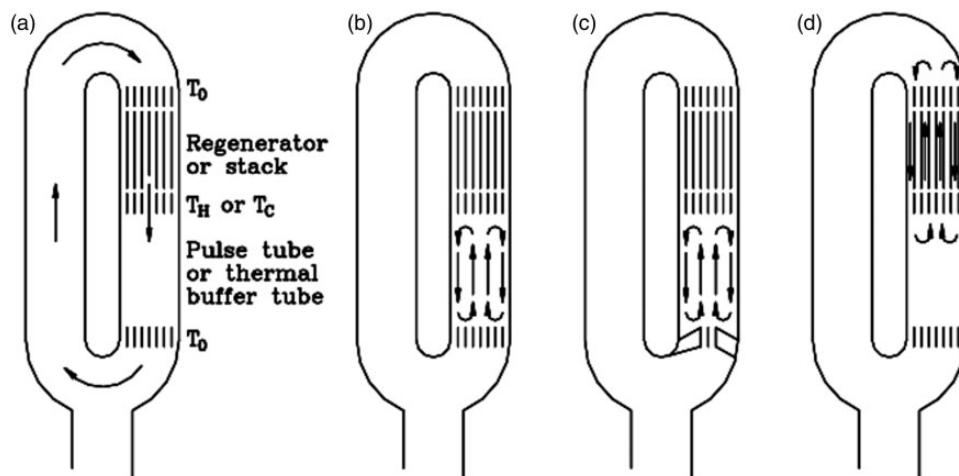


Figure 13. Main types of gas streaming in engines and refrigerators. (a) Gedeon streaming, (b) Rayleigh streaming, (c) jet-driven streaming, (d) streaming within the regenerator, from Swift,²⁵ reproduced with the permission of the Acoustical Society of America.

thermal buffer tube, thus degrading the temperature gradient in the regenerator. In practice, this suppression is achieved more or less empirically by means of jet-pumps¹⁷ membranes¹⁹ or tapered tubes.⁹² However, Penelet et al.⁹³ have shown that the amplification may actually be increased by the streaming through its influence on the shaping of the temperature field.

The presence of acoustic streaming may also impact the thermoacoustic process itself. Holzinger et al.⁹⁴ have computed the effect on the thermoacoustic conversion at low Mach numbers and find that the amplification is reduced relative to the no-flow case, so this is an additional reason for suppressing Gedeon streaming. However, Reid and Swift⁹⁵ have investigated devices in which the acoustic perturbations are deliberately superimposed on a mean flow, with the benefit that heat transfer surfaces may be eliminated.

- (c) Inherent limitation of the unsteady heat transfer processes when the amplitude of the acoustic velocity becomes large.

This mechanism is most readily apparent in flames, where curling of the flame front at high amplitudes often leads to interactions of different segments and quenching as they compete for the same fuel. In other cases, heat loss to the flame holder or other surfaces at high amplitudes can also give rise to non-linearity. In an engine, if the acoustic displacements are large in relation to the depth of a stack or regenerator, the time spent by the fluid outside the area of heat transfer will cause a similar loss of linear dependence on the acoustic velocity. A further source of non-linearity lies in the temperature field at the end of a stack, where the acoustic displacement takes gas into a heat exchanger. It is shown by Gusev et al.⁹⁶ that this leads to a peaking of the acoustic amplitudes at the end of the stack and that substantial thermal harmonics are generated; experimental evidence of this process has been provided by Berson et al.⁹⁷ and Penelet et al.⁹³

- (d) Limitation in the supply of heat to the thermoacoustic medium when the amplitude of the acoustic velocity becomes large.

Even if the exchange surfaces are deep enough for the acoustic displacements at the highest intensities to be sufficient for efficient heat transfer to the heat exchangers (at least two displacements deep), there is a possible limitation in the transfer to the secondary streams. There may not be sufficient heating or cooling capacity in those streams to maintain a temperature difference close to the maximum (i.e. that between the secondary streams) in the stack. The result is a

loss of the energy input to an acoustic travelling-wave, which is

$$W_{gen} \propto (T_h - T_c) |p|^2 \quad (38)$$

The non-linearity arises because the gas temperatures become functions of the acoustic intensity.

There is no obvious parallel in flames, since the fraction of the enthalpy of combustion converted to sound is extremely small: plenty more is available for all conceivable sound intensities.

In practice, limit cycling in practical combustion systems usually indicates a non-linearity in the flame response to acoustic velocities (process c), the acoustic processes remaining essentially linear (Figure 14(a)). On the other hand, the limit in engines is often due to the limited temperature difference between source and sink streams. The generation is linear in the acoustic intensity with a gradient dependent on the temperature difference, according to equation (38), until the temperature difference is reduced by acoustic streaming or inadequate heat transfer (processes b and d), as shown by the tendency to saturation of the 'generation with the highest temperature difference possible' in

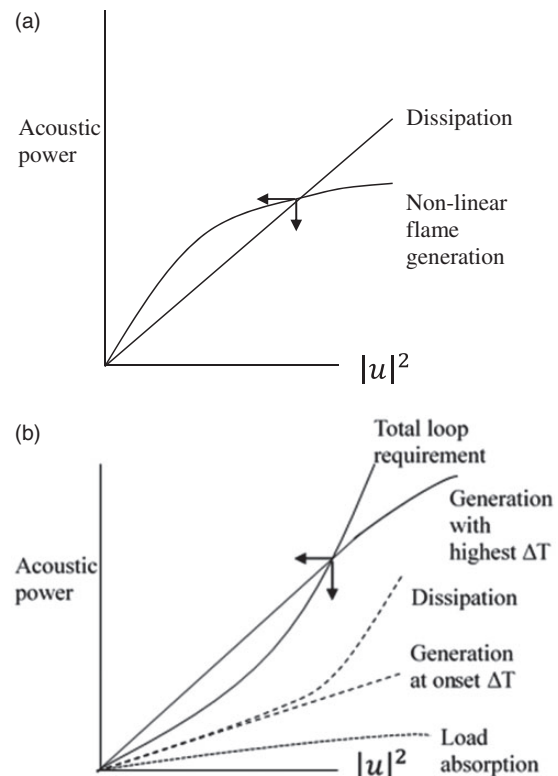


Figure 14. Determination of limit cycling in (a) flames and (b) engines in the most common situations. Total loop acoustic power requirement in engines is the sum of the dissipation and the load absorption.

Figure 14(b). However, it is the non-linear acoustic losses (process a), added to the load absorbed by say a linear alternator (also non-linear because of the limited stroke), that determines the acoustic intensity. (Note that the coincidence of the losses curve with the generation curve for a lower temperature difference determines the thermal conditions for onset of acoustic oscillations.)

4.6 Non-linear observations in flameless thermoacoustic devices

Limit cycling: The immediate and most obvious effect of a non-linearity is for the system to come to a ‘limit cycle’, the non-linearity reducing the energy generation or enhancing the dissipation, as has just been discussed. As mentioned earlier, Heckl⁸⁷ and Matveev⁸⁴ both consider that heat transfer from the grid in a Rijke tube is

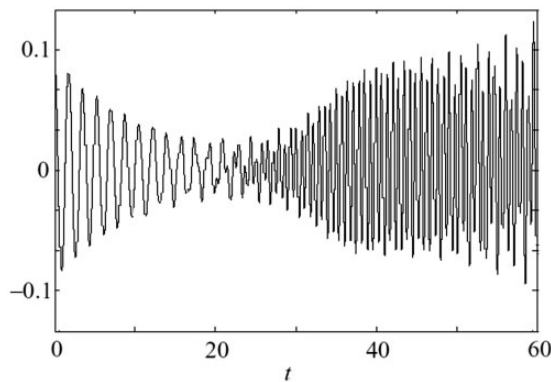


Figure 15. The evolution of acoustic velocity at the flame location with time in a Rijke tube, from Balusubramanian and Sujith,¹⁰¹ reproduced with the permission of Elsevier.

given by King’s law and is thus a function of the square root of the acoustic velocity, diminishing the energy generation relative to the dissipation as the intensity increases. This is actually closer to the usual situation with flame excitation (Figure 14(a)) than the normal engine situation (Figure 14(b)). In thermoacoustic engines, the acoustic intensity does not directly influence the proportional rate of heat released to the fluid. However, similar but indirect processes occur, since a reduction of the temperature gradient is caused by thermoacoustic streaming and acoustic streaming, and by limitations in the heating power that can be provided by the hot source.

Non-normality and triggering: Balusubramanian and Sujith,⁹⁸ Mariappan and Sujith⁹⁹ and Gopalakrishnan and Sujith¹⁰⁰ have explored the nature of the instability in more detail, identifying the role of the ‘non-normality’ of the governing equations (the non-orthogonality of the eigenvectors) in allowing growth while the individual eigenvectors decay. There is also the possibility of ‘triggering’, growth for some initial conditions, but not for others. Figure 15 shows a sequence in which there is initial decay of a low frequency oscillation, followed by growth and eventual limit cycling at a much higher frequency. The transitions are identified as being ‘sub-critical’ on a bifurcation diagram, a plot of some amplitude against some system parameter, with considerable hysteresis in the observations becoming possible (Figure 16).

Effect of mean flow: For the case where there is a mean flow, Mariappan and Sujith⁹⁹ performed an asymptotic analysis, expanding the variables in powers of Mach number, to obtain separate equation sets for the acoustic field and for the heater. A ‘global acceleration’ term appears in the heater zone and strongly affects the bifurcation diagram for the

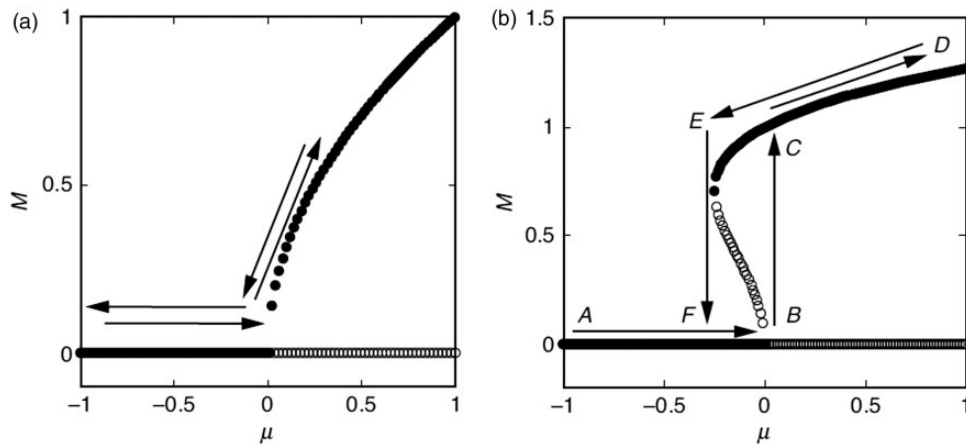


Figure 16. Bifurcation diagram depicting variation of a measure M with a control parameter μ . (a) Supercritical bifurcation and (b) subcritical bifurcation. From Gopalakrishnan and Sujith,¹⁰⁰ reproduced with permission of Sage Publications Ltd.

system. This term was also found by Moeck et al.¹⁰² in analysing a Rijke tube with a flame instead of the heated grid. Gopalakrishnan and Sujith¹⁰⁰ point to the effect of the acoustic streaming in shifting the experimentally determined bifurcation diagram with increasing heat transfer.

Periodic switching/pulsing/surging in engines: Complex behaviour is observed when variable rates of heat transfer are imposed: Penelet et al.¹⁰³ found that, depending on the process of heating, a ‘double threshold’ approach to stabilisation or a periodic switching on and off¹⁰⁴ are possible. Both processes were observed in a closed-loop, stack-based travelling wave engine, where Gedeon streaming is generated along the loop and impacts the temperature distribution in the stack and the thermal buffer tube. The experimental results for the regime of periodic switching are reproduced in Figure 17, where both acoustic pressure amplitude and the hot temperature are presented as a function of time. The results show spontaneous, periodic variations of both pressure and temperature (Figure 17(a) to (c)). It is also worth pointing out that, when the heating is sufficiently high that steady amplitude oscillations are obtained (Figure 17(d)), the steady-state value of the hot temperature T_H is lower by several tens of Kelvins than its value just before the

onset: this is a clear indication that the temperature difference along the stack is not sufficient to describe thermoacoustic amplification; otherwise, the steady-state hot temperature should be higher or equal to its value at threshold.

This was modelled numerically by including a Gedeon streaming velocity proportional to the acoustic intensity,¹⁰⁵ so that a substantial diminution in the temperatures at the hot end of the stack accompanying the rise in acoustic pressure, and a rise of temperature in the thermal buffer tube, are observed as the streaming convects thermal energy away from the stack. Similar behaviour has been computed by Scalo et al.⁶⁵ with full 3D CFD solutions for the configuration of Figure 18, one that had been investigated by Lycklama a Niejholt et al.¹⁰⁶ in an early application of CFD to non-linear thermoacoustic problems. Scalo et al.⁶⁵ found that the efficiency of this device falls with increases in the ratio of the temperatures across the regenerator, due to the streaming. However, as Gedeon streaming also impacts the shape of the temperature profile in the thermal buffer tube, it may affect significantly the process of wave amplification in the stack. Since the scattering of acoustic waves also depends on the temperature distribution in the thermal buffer tube, depending on the device under consideration, this modification of the

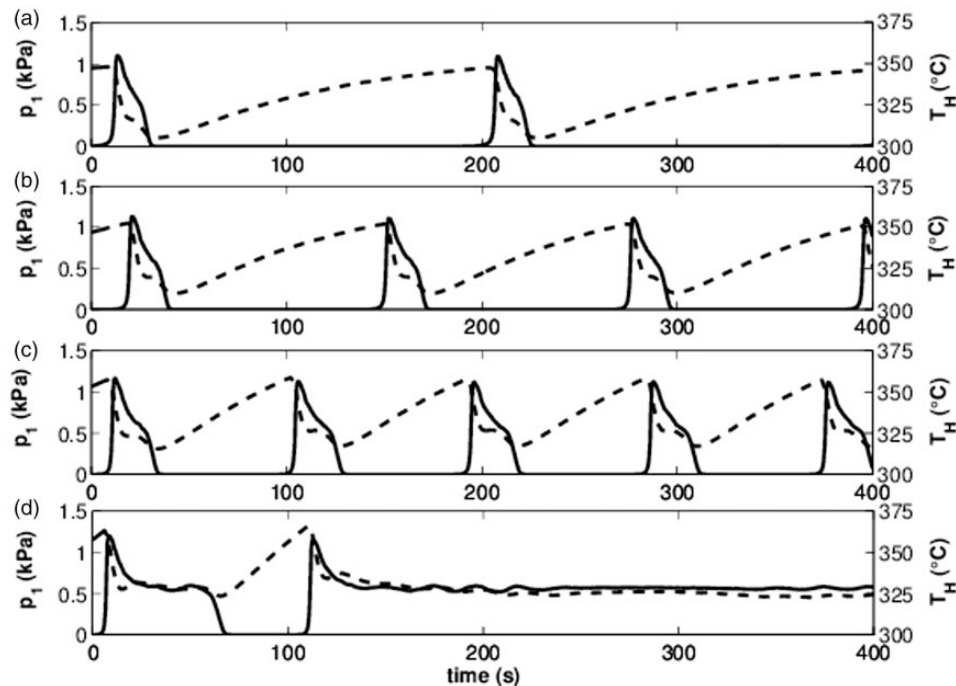


Figure 17. Evolution of the root-mean-square amplitude p_1 of acoustic pressure oscillations (solid line) and of the temperature at the hot stack end T_H (dashed line) as a function of time. The different figures correspond to different regimes of heating, namely to (a) $\Delta Q/Q_0 = 5\%$, (b) $\Delta Q/Q_0 = 10\%$, (c) $\Delta Q/Q_0 = 20\%$, and (d) $\Delta Q/Q_0 = 30\%$, where Q_0 corresponds to the threshold value of the heat supply above which self-sustained oscillations are generated, and where ΔQ corresponds to the increment in heat supply (e.g. in (a) a total amount of heat power $Q_0 + \Delta Q$ is supplied to the thermoacoustic system) (from Penelet et al.¹⁰⁴).

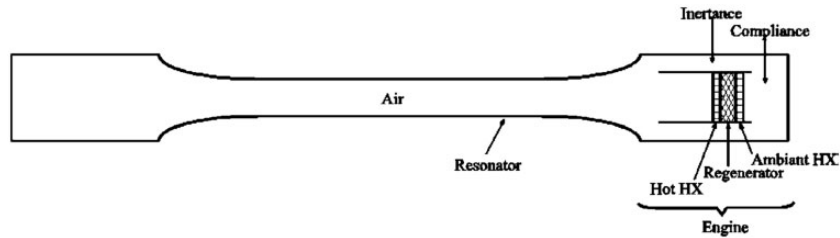


Figure 18. Schematic of a thermoacoustic engine with annular inertance, from Lycklama a Niejholt et al.,¹⁰⁶ reproduced with the permission of the Acoustical Society of America.

temperature profile can give rise to additional thermoacoustic amplification.¹⁰⁷

The process of periodic switching has also been reported in standing wave prime movers where Gedeon streaming is absent, but other types of streaming are present.¹⁰⁸ An example is presented in Figure 19 for the case of a quarter wavelength thermoacoustic prime-mover. Different regimes, depending on stack position and heat supply, all give rise to stable oscillation after the transient (which itself always involves an overshoot of wave amplitude growth) and are well reproduced by numerical simulations. However, the same device can also give rise to the onset (even after several minutes of stable oscillations) of a regime of periodic switching.

There are reports of periodic pulsing or surging in looped tube engines, and these are also associated with changes in temperature. Yu et al.¹⁰⁹ and Abduljalil et al.¹¹⁰ describe a ‘fishbone-like’ pressure instability trace (Figure 20) following start-up with intermediate levels of heat flux. The normal exponential growth in pressure amplitude is followed by a decay, before the sequence repeats at 14 to 17s intervals with increasing amplitude. Eventually, the amplitude saturates, decays rapidly and then reaches a stable quasi-steady state. Lawn found similar surging behaviour in a loop which has the additional complication of radiant heat transfer from a hot plate to the hot end of the regenerator.¹¹¹ The sudden onset of high-intensity pressure fluctuations leads to a rapid fall in all the temperatures at the hot end, with the gas in the hottest region dropping by some 260 K from 1060 K to 800 K (Figure 21). There are then changes in the temperature distribution in the loop, presumably because Gedeon streaming into the thermal buffer tube further degrades the heat available to the regenerator. In a successful start, the acoustic intensity settles, albeit at a somewhat lower level than the initial one, but more often, the intensity falls away over a period of about 30 s and the temperatures recover over 2–3 min, for the cycle to repeat indefinitely. In other experiments, more rapid surges over periods of 20–30 s were observed with variations at the hot end of the regenerator of only about 5 K, but of 150 K at the end of the thermal buffer tube. All of the

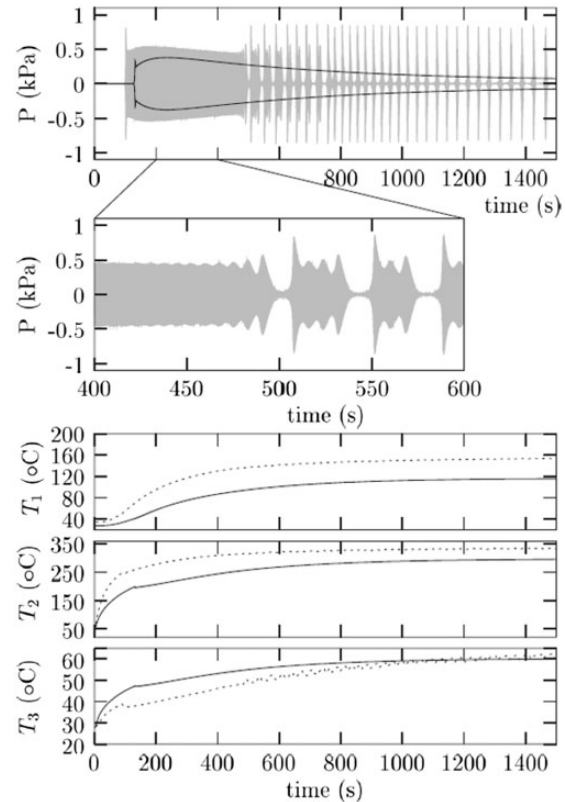


Figure 19. Transient regime of wave amplitude growth obtained in a quarter wave tube. Both the evolution of acoustic pressure and of some temperatures are presented as a function of time (T_1 : temperature in the middle of the stack, T_2 : temperature near the hot the stack end, T_3 : temperature measured 2.5 cm away from the hot stack end in the duct). Experimental results are presented with grey shading for acoustic pressure, and with dashed lines for the temperatures T_i . Theoretical results are presented with solid lines, from Guedra et al.¹⁰⁸

processes mentioned above are probably due to some complex interaction of sound amplification with heat transport by sound, but reproducing such dynamics with numerical simulation remains a challenging issue.

Quasi-periodic and chaotic oscillations: Thermoacoustic prime-movers are also an example of autonomous oscillators giving rise to some universal manifestations of

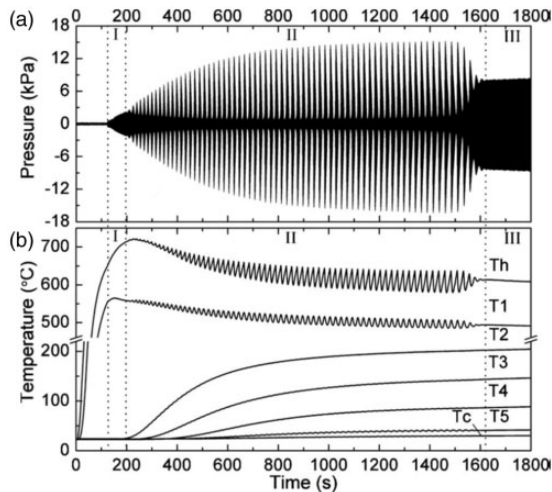


Figure 20. 'Fishbone-like instabilities in a thermoacoustic engine, from Yu et al.,¹⁰⁹ reproduced with the permission of the Acoustical Society of America.

dynamical systems, like quasi-periodicity, hysteresis or chaotic oscillations. More than 20 years ago, Yazaki¹¹² reported that Taconis oscillations (thermoacoustic oscillations observed at cryogenic temperatures) exhibit synchronization and chaotic dynamics when forced by external oscillations. The synchronisation of a standing-wave prime-mover by an external sound source was also studied by Penelet and Biwa,¹¹³ giving rise to the second experimental evidence of the phase-trapping process (see also Li and Juniper¹¹⁴ for more details). In a standing-wave engine, Unni et al.¹¹⁵ examined the relationship between heating power and the amplitude of pressure oscillations and found a range in which strong quasi-periodic oscillations occurred due to the beating of the fundamental with a higher frequency mode. This mode was favoured by the thermal penetration in the stack as the temperatures increased, until eventually there was limit cycling at the higher frequency. There was also hysteresis: the lower frequency mode was inhibited when the heat flux was reduced.

Shock waves and solitons. Although in most applications of thermoacoustic engine, the acoustic propagation can be reasonably described as linear, the cascade process of higher harmonics generation can, sometimes, lead to significant distortion of the wave at large amplitudes. This is notably the case in resonators with simple geometry (e.g. in straight duct or closed loop engines) in which higher order resonance frequencies are (almost) multiple integers of the fundamental one. This observation motivated fundamental studies of non-linear propagation in thermoacoustic engines in the early 2000s.^{116,117} More recently, the first experimental observation of thermoacoustic shock waves has been reported by Biwa et al.¹¹⁸ and reproduced numerically by Olivier et al.¹¹⁹ The autonomous

generation of a thermoacoustic solitary wave rotating along a 20 m long closed loop, with many Helmholtz resonators connected to it, has also been recently reported by Shimizu et al.¹²⁰

4.7 Non-linear observations in flames

In the last few years, many measurements have been made of the non-linear response of various types of flame. The linearity with respect to incident velocity perturbations of low amplitude has already been described earlier. For computation of non-linear effects, the processes are expressed in terms of an FDF, in which the amplitudes and phases of response are made functions of the acoustic velocity.

Limit cycling in ducted flames: Having explored the frequency response of ducted flames simulating jet engine afterburners in her 1995 paper, Dowling⁶⁸ showed that a simple model for the saturation of the heat release (process c) can give rise to limit cycling. Therefore, here it is assumed to be some limitation in the heat input to the gas that limits the amplitude, as in many thermoacoustic engines, but the mechanism is unspecified. The frequencies and mode shapes are barely affected by the non-linearity. In a later paper, Dowling⁸ developed a more physical model along the lines set out by Fleifel et al.⁶⁷ by calculating the effect of extreme perturbations on the motion of the flame front (Figure 22). The resulting limit cycle had an amplitude similar to that of experimental data.

Limit cycling in swirling flames: A large number of studies have also uncovered the non-linear behaviour of swirling flames of the type found in gas turbines and power station equipment. In general, it is found that, with increases in the amplitude of the air velocity oscillations to over 10% of the mean velocity, different areas of the flame front begin interacting with each other and the linearity is disrupted. Flame wrinkles become so severe that some of the front is closed off or shed vortices curl the flame back on itself and are extinguished (Figure 23). Another mechanism is described by Moeck et al.,¹²² who show that there is a helical mode which interacts non-linearly with the acoustic oscillations. From experiments with a full gas turbine combustor, Kim and Hochgreb¹²³ elucidate the approach to limit cycles in this geometry and explain these in terms of the non-linearity of the heat release relative to the dissipation as a function of the pressure amplitude (Figure 24). (Note that here it is the actual pressure amplitude that is being plotted, and not the power vs the square of the amplitude, as in Figure 14.)

Triggering: For a lean premixed combustor also with centre-body stabilisation, Lieuwen¹²⁴ identified a tendency for the pressure amplitude and frequency to increase with the mean inlet velocity. Significant

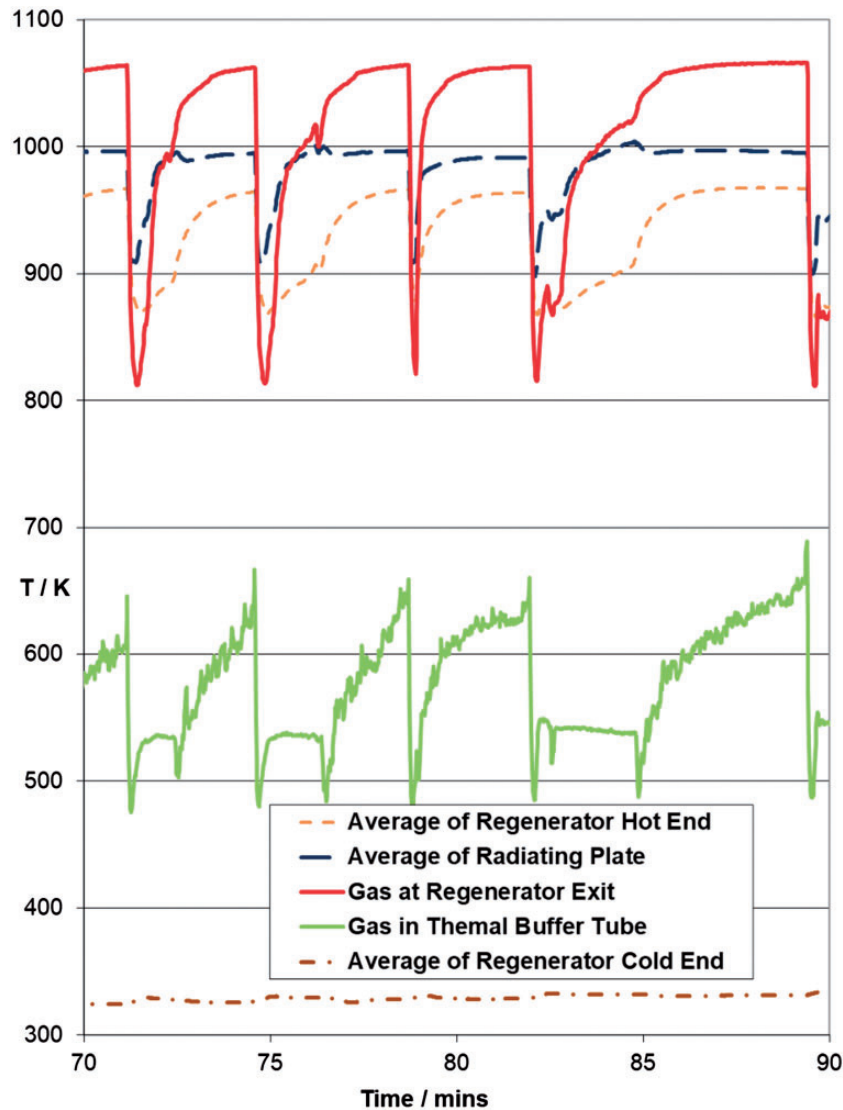


Figure 21. Effect on temperatures of the surging of high intensity oscillations in a radiatively heated thermoacoustic engine, described in Lawn.¹¹¹

non-linear interactions in the frequencies were observed at amplitudes well below that at which the pressure vs heat release departed from linearity.¹²⁵ Both subcritical and supercritical bifurcations could occur for the same system parameters, the former exhibiting the ‘triggering’ phenomenon that has already been noted for a Rijke tube.

Bootstrapping and effect of mean flow: Another form of stabilisation, that in a ‘dump combustor’ with a sudden expansion inducing the shedding of vortices in the incoming premixture, was studied by Matveev and Culick.¹²⁶ Their model for the shedding from the expansion edge involved a frequency and a vortex circulation based on a characteristic Strouhal number, and combustion within the vortex after a time

determined either by diffusion and chemistry, or by impingement on a downstream edge. Revisiting and simplifying the latter case, Tulsyan et al.¹²⁷ showed that the non-normality of the system led to some interesting effects, including ‘bootstrapping’, the transfer of energy between modes and back again, so that increased damping could actually give rise to greater amplitude. This effect was deemed responsible for the computed cycling of the amplitude over nine cycles or so (Figure 25). Further consideration of the effect of non-normality, particularly with a mean flow and a choked exit, was presented by Wieczorek et al.¹²⁸

Also for plane ducted flames, but with stabilisation on the recirculations induced by a sudden expansion, Kashinath et al.¹²⁹ used DNS and a ‘G-equation’

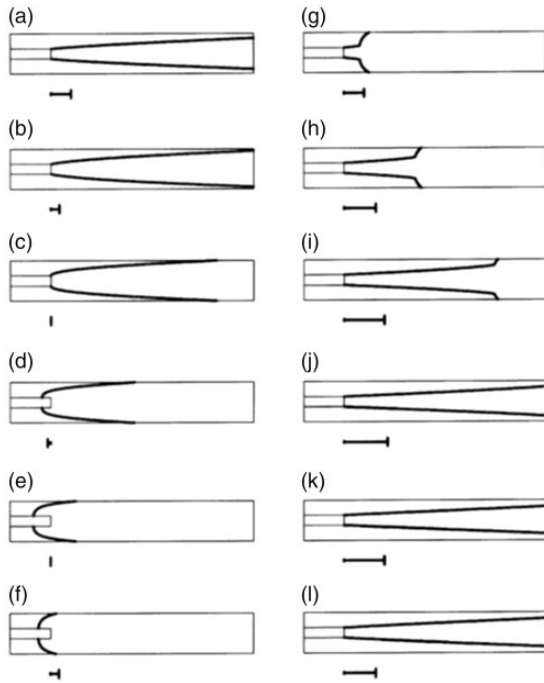


Figure 22. Calculated periodic fluctuations in the position of the flame surface for unsteady premixture inlet flow to a bluff-body stabilised combustor, from Dowling.⁸

describing the position of the flame front to show that, when the phase-speed of the acoustic waves does not equal the mean flow speed, the system supports multiple limit cycles, because the phase of the FDF changes significantly with oscillation amplitude. Increasing further the complexity of the flame, Han et al.¹³⁰ take results for a burner stabilised by a bluff-body and sudden expansion, and generate the FDF by LES. This prescription also yields limit cycles in good agreement in frequency and amplitude with the experimental data.

Hysteresis and mode switching: Noiray et al.¹³¹ and Boudy et al.¹³² show for a multi-point injection flame that, with the FDFs displayed in Figure 26, a variety of responses are possible, depending on the length of the feeding manifold. There may be linear instability giving rise to immediate limit cycling, or there may be linear stability followed by non-linear instability and limit cycling at higher amplitudes. Hysteresis and mode switching from one frequency to another very different one are also predicted and observed, as for the engines. Heckl¹³³ found that the qualitative stability behaviour of this burner can be predicted with amplitude-dependent coefficients in a generalised n - τ law with multiple time-lags.

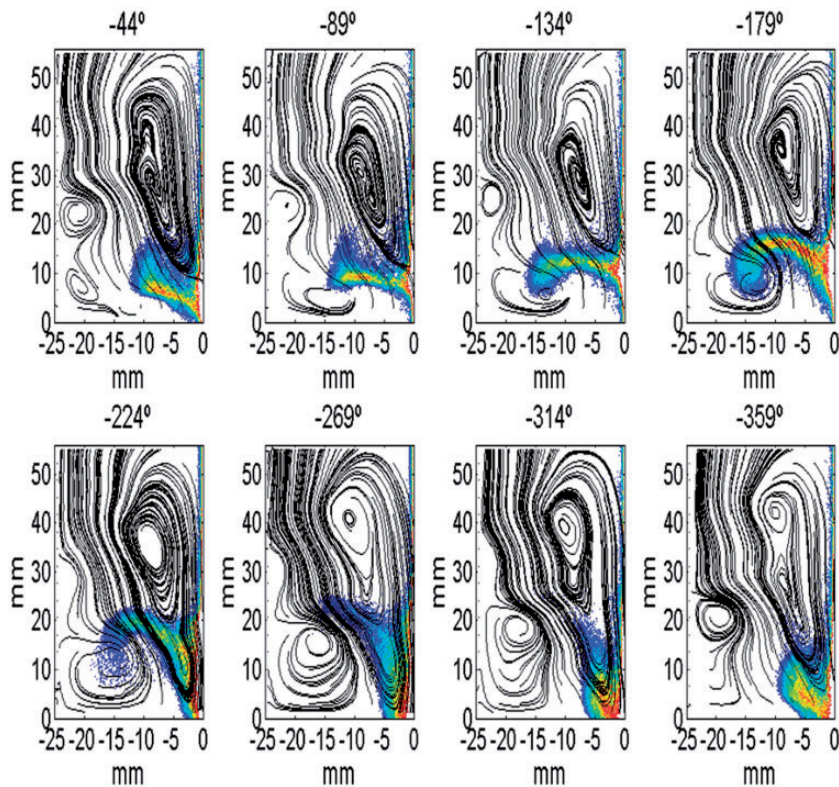


Figure 23. For a model gas turbine burner, the phase-locked, Abel de-convoluted, OH* intensity (shading) with velocity streamlines at eight phases with respect to the fluctuating velocity. 200 Hz, 31% r.m.s velocity fluctuations, $\phi = 0.56$, from Hosseini et al.⁴¹

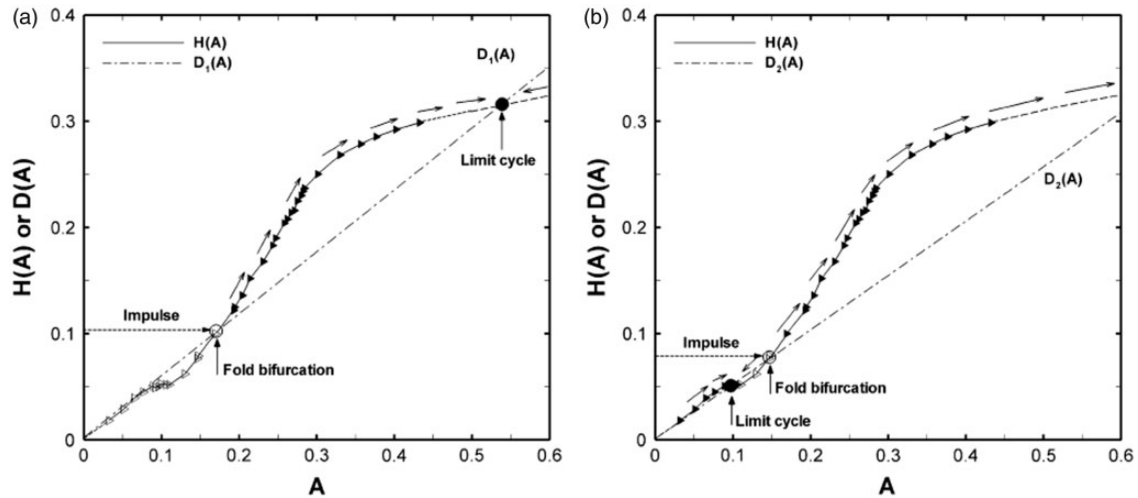


Figure 24. Amplitude dependence of flame describing function driving (H) and two damping (D) processes at a forcing frequency of 180 Hz in a gas turbine combustor are plotted against the forcing amplitude (A). Filled triangles, stable solutions; open triangles, unstable solutions; open circles, fold bifurcation; filled circles, stable limit cycles, from Kim and Hochgreb,¹²³ reproduced with the permission of Elsevier.

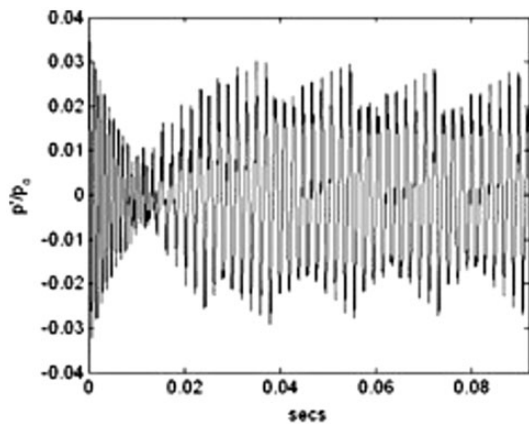


Figure 25. Computation of the effect of 'bootstrapping' in giving rise to amplitude cycling in a cavity-stabilised combustor, from Tulsyan et al.,¹²⁷ reproduced with the permission of Taylor and Francis.

Periodic switching/pulsing/surging in flames: In combustion, surging over periods of more than 10 s has been observed by one of the present authors (Lawn), but he can find no literature references. Where it occurs, the mechanism is probably similar to that described for thermoacoustic engines: one of changing temperature distribution in components with substantial thermal capacity. It may be associated with high-pressure amplitudes changing the mean flame configuration (e.g. lifting the flame) and the subsequent heating or cooling of the burner mouth changing the thermal radiation in such a way that the flame reverts to its original position. The position of the flame was artificially controlled by movement of a mesh in a spray combustor by Pawar

et al.¹³⁴ and they observed a progression from stable operation, through periodic bursts of high intensity at 10 s intervals, to shorter intervals, and finally to limit cycling, as the mesh was moved down the tube.

Quasi-periodic and chaotic oscillation: Quasi-periodic pulses about every 0.1 s have been observed by Hong et al.¹³⁵ in a dump combustor and shown to be associated with equivalence ratio fluctuations and the lifting of the premixed flame in a regime of mean equivalence ratio approaching that of lean blow-out. Also in that regime, Nair et al.,¹³⁶ Domen et al.¹³⁷ and Unni and Sujith¹³⁸ examine intermittency in pressure fluctuations on a similar timescale in a swirled combustor and proposed it as a diagnostic for blow-out. In these cases, the convection time from the pre-mixer to the flame is probably critical in determining the pulse periods where there was some regularity.

Shock waves: While shock waves are generally absent during combustion in air, the energy dissipation associated with them can be the dominant amplitude limiting mechanism in small solid rocket engines, as modelled by Greatrix.¹³⁹ Study of these phenomena could improve understanding of the engine observations previously discussed in Section 4.5.

5. Control of excitation

5.1 Passive control of engines through design

Since the objectives of control in thermoacoustic engines and flames are generally entirely different – to enhance the oscillations in the former and to suppress them in the latter – the techniques are generally

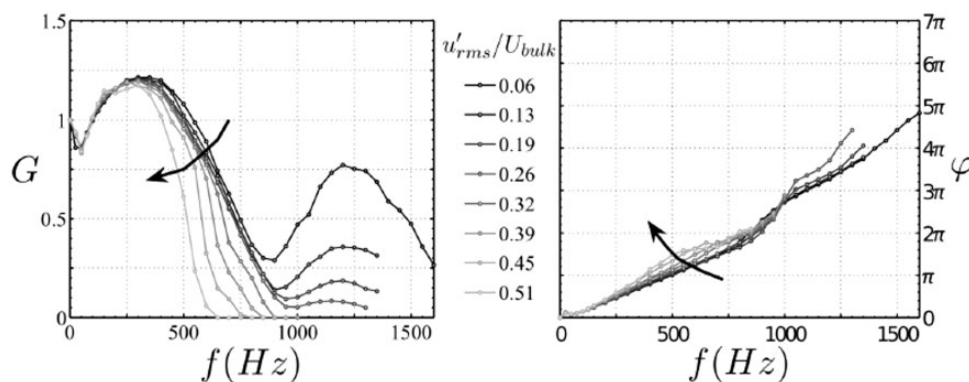


Figure 26. Measurements of the gain G and phase $P (= -\varphi)$ of the FDF as a function of the frequency and the input level for a multi-point injection flame, from Boudy et al.,¹³² reproduced with the permission of Elsevier.

different, but perhaps may be applied in a negative way to the other system.

For travelling-wave engines, there is a particular problem in the design stage of selecting the best regenerator material and placing the optimum depth in the best position in the loop. The selection has to balance the need for excellent thermal contact (δ_k large) against the enhanced dissipation if the passages are too small (r_h small). The trade-off will depend to some extent on the losses in the remainder of the loop, including those incurred in driving an alternator. Yu et al.¹⁴⁰ and Guedra et al.¹⁴¹ examine various types of regenerator material, such as stainless steel wire mesh, NiCr foam, ceramic catalyst and wire scrubbers. The optimum passage size in terms of the ratio of generation to dissipation for a given material depends on the temperature gradient and on the specific acoustic impedance of the acoustic wave in the regenerator.¹⁴²

Almost independently of the material, the optimum is between $r_h = \delta_k/3$ and $\delta_k/2$, slightly more than that giving the minimum temperature difference for onset, as determined by Yu et al.¹⁴³ The greatest possible temperature gradient demands a small depth of regenerator but leads to high conduction losses, and it is this that determines the optimum depth.

For the standing-wave engine or refrigerator, Babaei and Siddiqui⁵⁰ apply parametric variation in their own thermoacoustic model to predict the optimum length of the engine and the position of the stack within it, from the point of view of the thermal efficiency or the coefficient of performance, respectively. In a similar analysis for standing-wave prime movers, Nouh et al.¹⁴⁴ use calculations with DeltaE to determine the optimum stack position for a variable area resonator, the results being relatively insensitive to the stack length. With helium at 10 bar, the plate spacing for maximum efficiency was 2.4 times the thermal penetration depth in this case. The analysis, experiments and DeltaE calculations of Tijani et al.²⁴ for a refrigerator with a buffer

volume under these conditions give $3\delta_k$ as the value for maximum cooling power. Thus, the optimum is some eight times that for a travelling wave device.

A method of using the scattering matrix (equation (20)) to optimise the boundary conditions of a regenerator has been outlined by Holzinger et al.⁵² This method is at least of theoretical interest in trying to assess mechanisms of intrinsic instability in flames,^{43,44} although measurements on the hot gases downstream are difficult. It was shown by Lawn¹⁴⁵ that the required levels of accuracy in the measurement of regenerator transfer functions are demanding, and hence useful results for the optimum input and output impedances are difficult to achieve.

Hatori et al.¹⁴⁶ measured the impedance of a complete loop containing a regenerator from a side branch, and then matched it with the impedance of an acoustic load characterised in a separate experiment with propagation in the opposite direction. The same approach has been successfully employed by Yahya et al.¹⁴⁷ in matching two acoustic drivers to a looped thermoacoustic refrigerator through an inertance tube and a capacitance in front of the driver diaphragms. The necessary dimensions for capacitive and inertance elements can be calculated accurately enough by analytical methods, but for engines and refrigerators the program DeltaEC is often employed.

There is no equivalent standard procedure for flames, where in any case, the scope for geometric modifications to actual equipment is likely to be more restricted.

5.2 Passive control of flames

Nevertheless, for combustion systems, the concern to damp the possible frequencies of excitation has led to experiments in which the capacitance property is used in a different way. By expanding the premixture inlet section on their burner, Bellucci et al.¹⁴⁸ effectively

formed a Helmholtz resonator and tuned out the predominant mode so that the pressure amplitude of thermoacoustic excitation by the flame was reduced by 50%. For a broader spectrum of sound absorption, the use of a perforated liner in the inlet tube, with the premixture flowing through the holes at about Mach 0.03, has also been shown by Tran et al.¹⁴⁹ to be effective on a test rig, in line with theory developed by Eldridge and Dowling.¹⁵⁰ Lahiri et al.¹⁵¹ conducted absorption experiments over a wider range of geometries, some with double cavities and grazing flow, and Lahiri and Bake¹⁵² provide a comprehensive review of the available theories and experimental data for absorption by orifices with both bias (through-) flow and grazing flow. Lawn¹⁵³ successfully modelled a range of Lahiri's results. These included the observation that greater than 50% absorption could be obtained over a range of frequencies with relatively large (2.5 mm diameter) orifices and very small bias flow. (Higher bias flow may be required if the absorption function is integrated with that of cooling the liner of the actual combustion chamber.) Such absorptive linings could conceivably find applications at the extremities of thermoacoustic engines in suppressing the noise radiated to the environment.

In annular combustion chambers with azimuthal modes, other options are available. Worth and Dawson¹⁵⁴ found that three or more baffles were required to achieve significant damping, while Parmentier et al.¹⁵⁵ examined analytically the effect of mixing two different types of burner around the annulus.

In addition to these modifications to the acoustic boundary conditions of the flame, there may also be the option of modifying the flame itself, perhaps by modifying the shear layers on which it is stabilised.¹⁵⁶ In the case of the oil burner problem mentioned in the Introduction section,¹⁰ modification of the swirler to a more open design, with blades cut back near the hub, ventilated the internal recirculation zone and favourably shifted the operational region of instability. Alternatively, the structure of the flame may be modified by changing the nature of the fuel. A mixture of methane and ethane, dilution by N₂ and changes to the premixture, all changed the crucial time delay in a pulse combustor.

5.3 Active control of flames

Active control implies using a sensor such as a microphone to detect an instability, and then feeding-back the signal to control some kind of actuator to suppress the oscillation. The first application was to the suppression of reheat buzz by Bloxsidge et al.¹⁵⁷ The possibility was also discussed for a Rijke tube by Heckl.¹⁵⁸

Although there is some anxiety in the gas turbine industry about the disastrous consequences of the failure of an active control system to suppress high intensities, there is a considerable body of literature on laboratory demonstrations of the principle. Candel¹⁵⁹ reviews some possible strategies, particularly those for rocket motors. Gaseous fuel flows may be modulated up to about 400 Hz, with the injection timing carefully controlled to negate the natural instabilities. Fuel injection into four secondary flames was used by Sato et al.¹⁶⁰ to suppress pressure oscillations in a laboratory lean premixed combustor by 10 dB, for example. They also explored the secondary injection of air, with promising results.

With the rather different objective of manipulating the acoustic boundary conditions on a burner test rig to mimic those in operation in a combustion chamber, Bothien and Paschereit¹⁶¹ installed an electro-pneumatic transducer with a non-linear response on the burner flue duct. They found that quasi-arbitrary boundary conditions could be generated by adjusting the control law, thus allowing a wide range of conditions to be tested.

5.4 Active control of engines

Application of active control to thermoacoustic engines is less common. However, Olivier et al.¹⁶² have attached an additional acoustic source to the loop of a TASHE. The source was connected through a feedback loop to a reference microphone in the loop, a phase-shifter and an audio amplifier. As the amplifier gain was turned up, some net gain (or loss, and even quenching, depending on the assigned phase-shift on the feedback loop) in electrical power was recorded, probably brought about either by a modification of the acoustic field within the regenerator, or by a modification in the temperature field due to streaming. Many of the active control principles used to suppress excitation by flames in gas turbine systems in the laboratory should have application in engines to enhance the excitation.

6. Conclusion

The authors hope that this outline review of the principles and techniques that are deployed in studying the thermoacoustic instabilities generated by flames, alongside those for thermoacoustic engines, will stimulate some transfer of ideas between the two that we have not thought of. However, it has already been explained that there are some areas where inspiration might be sought in the literature of the other discipline. These include:

- (a) *The description of the process of heat transfer to the gas by a time-delay and the effect of this on the*

efficiency of the conversion to acoustic energy. This approach is indeed usual for flames and Rijke tubes, but much less so for thermoacoustic engines, for which the governing equations are usually derived in the frequency domain. This is probably due to the fact that, in the time domain, Rott's equations become integro-differential equations which are complicated to solve. However, the derivation of simplified equations in the time domain could open the way to a treatment of thermoacoustic engines from the standpoint of dynamical systems.

- (b) *The modelling of the acoustics of ducts surrounding the thermoacoustic source and their coupling with the source term.* Although in both combustion equipment and thermoacoustic engines, the problem often simply reduces to the description of plane waves (possibly with thermo-viscous losses, mean flow and/or temperature gradients), it is noticeable from the literature that the way they are treated in each discipline is often different. However, some of the experimental techniques for determining the relevant impedances in situ could have application to the other discipline.
- (c) *The empirical characterisation of elements of the acoustic path by transfer functions and scattering functions, and the optimisation of the impedance for the desired performance.* In particular, the extension of the FDF approach for the analysis of the dynamics of thermoacoustic engines would be interesting.
- (d) *The understanding of the Rijke tube, for which an accurate description of saturation processes remains an issue for both flame and heated gauze varieties.* The treatment of the temperature distribution, radiation end losses, and non-linear effects will be similar.
- (e) *The non-linear and non-normal behaviour of combustion and engine systems, including limit cycling, triggering, hysteresis and surging due to thermal effects.* The amplitude of cycling in a prime-mover engine tends to be limited by the available heat source, whereas that in a flame is often limited by the scope for increased flame area with high acoustic velocities. The most important difference between the two systems is perhaps the absence of a mean flow in most engines, until Gedeon streaming becomes important. Although this streaming flow remains much smaller in relation to the acoustic velocities than in a flame, it can provide a mechanism for periodic surging of the excitation.
- (f) *Active control, particularly instrumentation and algorithms.* The choice of control sources and their coupling with the system is important

for thermoacoustic engines and combustion systems.

Finally, although some effort has been made in this manuscript to emphasise common aspects between thermoacoustic engines and combustion-driven thermoacoustic instabilities, it must be remembered that an important difference lies in the fact that in the engine case, large amplitude oscillations are wanted, while in the combustion case, any oscillations are undesirable.

Acknowledgement

Our thanks are due to the Editor, Professor Wolfgang Polifke, for suggesting that a review of the two disciplines alongside one another would be useful, and to the referees for a number of helpful suggestions and criticisms.

Declaration of Conflicting Interests

The author(s) declared no potential conflicts of interest with respect to the research, authorship, and/or publication of this article.

Funding

The author(s) received no financial support for the research, authorship, and/or publication of this article.

References

- Higgins B. On the sound produced by a current of hydrogen gas passing through a tube, by Mr. Nicholson (Ed.) with a letter by Higgins regarding the time of its discovery. *J Nat Phil Chem Arts* 1802; 1: 129.
- Ueda Y. Kibitsuno Rohre Entkama – instrument used in historical Japanese shrine ritual. In: *2nd international workshop on thermoacoustics*, Sendai, Japan, 23–25 May 2014.
- Sondhauss C. Über die Schallschwingungen der Luft in erhitzten Glasrohren und in gedeckten Pfeifen von ungleicher Weite. *Ann Phy* 1850; 79: 1.
- Taconis KW, Beenakker JJM, Nier AOC, et al. Measurements concerning the vapour-liquid equilibrium of solutions of He³ in He⁴ below 2.19°K. *Physica* 1949; 15: 733–739.
- Rijke PL. Notiz über eine neue Art, die in einer an beiden Enden offenen Rohre enthaltene Luft in Schwingungen zu versetzen. *Ann Phys* 1859; 107: 339.
- Putnam AA, Belles FE and Kentfield JAC. Pulse combustion. *Prog Eng Comb Sci* 1986; 12: 43–79.
- Culick FEC. Unsteady motions in combustion chambers for propulsion systems. RTO-AG-039, RTO AGAR Dograph, 2006.
- Dowling A. A kinematic model of a ducted flame. *J Fluid Mech* 1999; 394: 51–72.
- Putnam AA. *Combustion-induced oscillations*. Ohio, USA: Battelle Institute, 1971.

10. Lawn CJ. *Principles of combustion engineering for boilers*. Orlando, FL: Academic Press, 1987, pp.42–45 and 189–191.
11. Huang Y and Yang V. Dynamics and stability of lean-premixed swirl-stabilized combustion. *Prog Energy Combust Sci* 2009; 35: 293–264.
12. Benoit JA, Ellis C and Cook J. Ultralow emission combustion and control system installation into mature power plant gas turbine. *ASME J Eng Gas Turbines Power* 2011; 133: 024001.
13. Ceperley PH. A pistonless Stirling engine – the travelling wave heat engine. *J Acoust Soc Am* 1979; 66: 1508–1513.
14. Swift GW. Analysis and performance of a large thermoacoustic engine. *J Acoust Soc Am* 1992; 92: 1551–1563.
15. Wheatley J, Hofler T, Swift GW, et al. Experiments with an intrinsically irreversible acoustic heat engine. *Phys Rev Lett* 1983; 50: 499–501.
16. Yazaki T, Iwata A, Maekawa T, et al. Travelling wave thermoacoustic engine. *Phys Rev Lett* 1998; 81: 3128–3131.
17. Backhaus S and Swift GW. A thermoacoustic-Stirling heat engine: detailed study. *J Acoust Soc Am* 2000; 107: 3148–3166.
18. Backhaus S, Tward E and Petach M. A traveling wave thermoacoustic electric generator. *Appl Phys Lett* 2004; 85: 1085–1087.
19. Tijani MEH and Spoelstra S. A high performance thermoacoustic engine. *J Appl Phys* 2011; 110: 093519.
20. Yu Z, Jaworski AJ and Backhaus S. A low cost electricity generator for rural areas using a travelling-wave looped-tube thermoacoustic engine. *Proc IMechE Part A, J Power Energy* 2010; 224: 787–795.
21. Richardson RN and Evans BE. A review of pulse tube refrigeration. *Int J Refrig* 1997; 20: 367–373.
22. Gifford WE and Longworth RC. Pulse tube refrigeration progress. *Adv Cryogenic Eng* 1964; 10B: 69.
23. Ueda Y, Mehdi BH, Tsuji K, et al. Optimisation of the regenerator of a travelling-wave thermoacoustic refrigerator. *J Appl Phys* 2010; 107: 034901.
24. Tijani MEH, Zeegers JCH and deWaale ATAM. Construction and performance of a thermoacoustic refrigerator. *Cryogenics* 2002; 42: 59–66.
25. Swift GW. *Thermoacoustics: a unifying perspective for some engines and refrigerators*. New York: Acoustical Society of America, American Institute of Physics Press, 2002.
26. Riley P and Lawn CJ. Low-cost, electricity generating heat engines for rural areas. *Proc IMechE Part A, J Power Energy* 2013; 227: 714–716.
27. deBlok CM. Low operating temperature integral thermoacoustic devices for solar cooling and waste heat recovery. *J Acoust Soc Am* 2008; 123: 3541.
28. Adef JJA and Hofler TJ. Design and construction of a solar-powered, thermoacoustically driven, thermoacoustic refrigerator. *J Acoust Soc Am* 2000; 107: L37–L42.
29. Garrett SL, Adef JJA and Hofler TJ. Thermoacoustic refrigeration for space applications. *J Thermophys Heat Transfer* 1993; 7: 595–599.
30. Owczarek P and deBlok CM. Details and experimental results of a stand-alone container cooled by a solar-driven multi-stage travelling wave thermoacoustic system. In: *Proceedings of the 3rd international workshop on thermoacoustics*, University of Twente, Netherlands, 26–27 October 2015.
31. Rayleigh WS. The explanation of certain acoustical phenomena, *Lecture at the Royal Institution*, 25 March 1878, and *Nature* 1878; 18: 319–321.
32. Merk HJ. An analysis of unstable combustion of premixed gases. *Symp (Int) Combust* 1956; 6: 500–512.
33. Dowling A. The calculation of thermoacoustic oscillations. *J Sound Vibr* 1995; 180: 557–581.
34. Chen LS, Bomberg S and Polifke W. Propagation and generation of acoustic and entropy waves across a moving flame front. *Combust Flame* 2016; 166: 170–180.
35. Baade PK. Design criteria and models for preventing combustion. In: *ASHRE symposium on combustion-driven oscillations*, Atlanta, 29 January 1978.
36. Mugridge BD. Combustion-driven oscillations. *J Sound Vibr* 1980; 70: 437–452.
37. Lawn CJ. Criteria for acoustic pressure oscillations to be driven by a diffusion flame. *Symp (Int) Combust* 1982; 19: 237–244.
38. Lieuwen TC. *Unsteady combustor physics*. New York: Cambridge University Press, 2012.
39. Lawn CJ and Polifke W. A model for the thermoacoustic response of a premixed swirl burner, part II: the flame response. *Combust Sci Tech* 2004; 176: 1359–1390.
40. Komarek T and Polifke W. Impact of swirl fluctuations on the flame response of a perfectly premixed swirl burner. *J Eng Gas Turbines Power* 2010; 132: 061503.
41. Hosseini SMR, Gardner C and Lawn CJ. The non-linear thermoacoustic response of a small-scale burner. *Combust Flame* 2012; 159: 1909–1920.
42. Zellhuber M, Schwing J, Schuermans B, et al. Experimental and numerical investigation of thermoacoustic sources related to high frequency instabilities. *Int J Spray Combust Dyn* 2014; 6: 1–34.
43. Hoeijmakers PGM, Kornilov VN, Lopez Arteaga I, et al. Intrinsic instability of flame-acoustic coupling. *Combust Flame* 2014; 161: 2860–2867.
44. Emmert T, Bomberg S and Polifke W. Intrinsic thermoacoustic instability of premixed flames. *Combust Flame* 2015; 162: 75–85.
45. Lawn CJ. Assessment of the performance of regenerators in travelling-wave thermoacoustic engines. In: *19th international congress on sound and vibration*, Vilnius, Lithuania, 8–12 July 2012.
46. Keller JO, Bramlette TT, Dec JE, et al. Pulse combustion: the importance of characteristic times. *Combust Flame* 1989; 75: 33–44.
47. Rott N. Damped and thermally-driven acoustic oscillations in wide and narrow tubes. *Z Agnew Math Phys* 1969; 20: 230–243.
48. Ward B, Clark J and Swift GW. Design environment for low-amplitude thermoacoustic energy conversion, DeltaEC., LA-CC-01-13.
49. Lawn CJ. Computational modelling of a thermoacoustic travelling wave engine. *Proc IMechE Part A, J Power Energy* 2013; 227: 783–802.

50. Babaei H and Siddiqui K. Design and optimisation of thermoacoustic devices. *Energy Conver Manage* 2008; 49: 3585–3598.
51. Guedra M, Penelet G, Lotton P, et al. Theoretical prediction of the onset of thermoacoustic instability from the experimental transfer matrix of a thermoacoustic core. *J Acoustic Soc Am* 2011; 130: 145–152.
52. Holzinger T, Emmert T and Polifke W. Optimizing thermoacoustic regenerators for maximum amplification of acoustic power. *J Acoust Soc Am* 2014; 136: 2432–2440.
53. Bannwart FC, Penelet G, Lotton P, et al. Measurement of the impedance matrix of a thermoacoustic core: application to the design of thermoacoustic engines. *J Acoust Soc Am* 2013; 133: 2650–2660.
54. Schuermans B, Guethe F, Pennell D, et al. Thermoacoustic modelling of a gas turbine using transfer functions measured under full engine pressure. *J Eng Gas Turbines Power* 2010; 132: 111503.
55. Palies P, Durox D, Schuller T, et al. The combined dynamics of swirler and turbulent premixed swirling flames. *Combust Flame* 2010; 157: 1698–1717.
56. Mejia D, Miguel-Brebion M and Selle L. The experimental determination of growth and damping rates for combustion instabilities. *Combust Flame* 2016; 169: 287–296.
57. Lamraoui A, Richecoeur F, Schuller T and Ducruix S. A methodology for on the fly acoustic characterisation of feeding line impedances in a turbulent swirled combustor. *J Eng Gas Turbines Power* 2011; 133: 011504.
58. Kosztin B, Heckl M, Muller R, et al. Thermoacoustic properties of a burner with axial temperature gradient. *Int J Spray Combust Dyn* 2013; 5: 67–84.
59. Blimbaum J, Zanchetta M, Akin T, et al. Transverse to longitudinal acoustic coupling processes in annular combustion chambers. *Int J Spray Combust Dyn* 2012; 4: 275–298.
60. Bauerheim M, Parmentier J-F, Salas P, et al. An analytical model for azimuthal thermoacoustic modes in an annular chamber fed by an annular plenum. *Combust Flame* 2014; 161: 1374–1389.
61. Camporeale SM, Fortunato B and Campa G. A finite-element method for three-dimensional analysis of thermoacoustic combustion instability. *J Eng Gas Turbines Power* 2011; 133: 011506.
62. Wolf P, Staffelbach G, Gicquel LYM, et al. Acoustic and large eddy simulation studies of azimuthal modes in annular combustion chambers. *Combust Flame* 2012; 159: 3398–3413.
63. Poignand G, Lotton P, Penelet G, et al. Thermoacoustic, small-cavity excitation to achieve optimal performance. *Acta Acust* 2011; 97: 926–932.
64. Smith RWM, Poese ME, Garrett SL, et al. Thermoacoustic device, US Pat. No. 6,725,670, USA, 2004.
65. Scalo C, Lele S and Hesselink L. Linear and non-linear modelling of a theoretical travelling-wave thermoacoustic heat engine. *J Fluid Mech* 2015; 766: 368–404.
66. Crocco L. Theoretical studies on liquid-propellant rocket instability. *Symp (Int) Combust* 1965; 10: 1101–1128.
67. Fleifil M, Annaswamy AM, Ghoniem ZA, et al. Response of a laminar premixed flame to flow oscillations: a kinematic model and thermoacoustic instability results. *Combust Flame* 1996; 106: 487.
68. Dowling A. Nonlinear self-excited oscillations of a ducted flame. *J Fluid Mech* 1997; 346: 271–290.
69. Polifke W and Lawn CJ. On the low frequency limit of flame transfer functions. *Combust Flame* 2007; 151: 437–451.
70. Ducruix S, Durox D and Candel S. Theoretical and experimental determinations of the transfer function of a premixed laminar flame. *Proc Combust Inst* 2000; 28: 765–773.
71. Leandro RE and Polifke W. Low-order modelling of distributed heat release. In: *19th international congress of sound and vibration*, Vilnius, 8–12 July 2012.
72. Arnott WP, Bass HE and Raspet R. Generalised formulation of thermoacoustics for stacks having arbitrarily shaped cross-sections. *J Acoust Soc Am* 1991; 90: 3228–3237.
73. Wilen LA. Dynamic measurements of the thermal dissipation function of reticulated vitreous carbon. *J Acoust Soc Am* 2001; 109: 179–184.
74. Swift GW and Ward WC. Simple harmonic analysis of regenerators. *J Thermophys Heat Transfer* 1996; 10: 652–662.
75. Lawn CJ. Acoustic pressure losses in woven-screen regenerators. *Appl Acoust* 2014; 77: 42–48.
76. Sugimoto N. Thermoacoustic-wave equations for gas in a channel and a tube subject to temperature gradient. *J Fluid Mech* 2010; 658: 89–116.
77. Swift GW. Thermoacoustic engines. *J Acoust Soc Am* 1988; 84: 1145–1180.
78. Tominaga A. Thermodynamic aspects of thermoacoustic theory. *Cryogenics* 1995; 35: 427–440.
79. El-Rahman A and Abdel-Rahman E. Computational fluid dynamics simulation of a thermoacoustic refrigerator. *J Thermophysics Heat Transfer* 2014; 28: 78–86.
80. Olsen JR and Swift GW. Similitude in thermoacoustics. *J Acoust Soc Am* 1994; 95: 1405–1412.
81. Tijani MEH, Zeegers JCH and deWaele ATAM. Prandtl number and thermoacoustic refrigerator. *J Acoust Soc Am* 2002; 112: 134–143.
82. Raspet R, Slaton WV and Hickey CJ. Theory of inert gas-condensing vapour thermoacoustics: propagation equation. *J Acoust Soc Am* 2002; 112: 1414–1422.
83. Raun RL, Beckstead MW, Finlinson JC, et al. Review of Rijke tubes, Rijke burners and related devices. *Prog Energy Combust Sci* 1993; 19: 313–364.
84. Matveev K. *Thermoacoustic instabilities in the Rijke tube: experiments and modelling*. PhD Thesis, California Institute of Technology, USA, 2003.
85. Kwon Y-P and Lee B-H. Stability of the Rijke thermoacoustic oscillation. *J Acoust Soc Am* 1985; 78: 1414–1420.
86. Torczynski JR and O'Hern TJ. Reynolds number dependence of the drag coefficient for laminar flow through electrically-heated photoetched screens. *Exp Fluids* 1995; 18: 206–209.
87. Heckl M. Non-linear effects in the Rijke tube. *Acustica* 1990; 72: 63–71.

88. Lawn CJ. The acoustic impedance of perforated plates under various flow conditions relating to combustion chamber liners. *Appl Acoust* 2016; 106: 144–154.
89. Olsen JR and Swift GW. Energy dissipation in oscillating flow through straight and coiled pipes. *J Acoust Soc Am* 1996; 100: 2123–2131.
90. Hossain MM, Malek MI, Ehsan M, et al. Score-stove performance with modified resonating tube shape and layouts. *International Conference on Mechanical Engineering*, Dhaka, Bangladesh, 27 December 2015, Paper 563.
91. Boluriaan S and Morris PJ. Acoustic streaming: from Rayleigh to today. *Int J Aeroacoust* 2003; 2: 255–292.
92. Olson JR and Swift GW. Acoustic streaming in pulse-tube refrigerators: tapered pulse tube. *Cryogenics* 1997; 37: 769–776.
93. Penelet G, Leclercq M, Wassereau T, et al. Measurement of density fluctuations using digital holographic interferometry in a standing wave thermoacoustic oscillator. *Exp Therm Fluid Sci* 2016; 70: 176–184.
94. Holzinger T, Baumgartner A and Polifke W. A quasi-one dimensional model of thermoacoustics in the presence of mean flow. *J Sound Vibr* 2015; 335: 204–228.
95. Reid R and Swift GW. Experiments with a through-flow thermoacoustic refrigerator. *J Acoust Soc Am* 2000; 108: 2835–2842.
96. Gusev V, Lotton P, Baillet H, et al. Thermal wave harmonics generation in the hydrodynamical heat transport in thermoacoustics. *J Acoust Soc Am* 2001; 109: 84–90.
97. Berson A, Poignand G, Blanc-Benon P, et al. Nonlinear temperature field near the stack ends of a standing-wave thermoacoustic refrigerator. *Int J Heat Mass Transfer* 2011; 54: 4730–4735.
98. Balusubramanian K and Sujith RI. Thermoacoustic instability in a Rijke tube: non-normality and nonlinearity. *Phys Fluids* 2008; 20: 044103.
99. Mariappan S and Sujith RI. Modelling non-linear thermoacoustic instability in an electrically heated Rijke tube. *J Fluid Mech* 2011; 689: 511–533.
100. Gopalakrishnan EA and Sujith RI. Influence of system parameters on the hysteresis characteristics of a horizontal Rijke tube. *Int J Spray Combust Dyn* 2014; 6: 293–316.
101. Balusubramanian K and Sujith RI. Non-normality and nonlinearity in combustion-acoustic interaction in diffusion flames. *J Fluid Mech* 2008; 594: 29–57.
102. Moeck JP, Schmidt H, Oevermann M, et al. An asymptotically motivated hydrodynamic-acoustic two-way coupling for modelling thermoacoustic instabilities in a Rijke tube. In: *ICSV 14*, Cairns, Australia, 9–12 July 2007.
103. Penelet G, Gaviot E, Gusev V, et al. Experimental investigation of transient nonlinear phenomena in an annular thermoacoustic prime-mover: observation of a double-threshold effect. *Cryogenics* 2002; 42: 527–532.
104. Penelet G, Gusev V, Lotton P, et al. Nontrivial influence of acoustic streaming on the efficiency of annular thermoacoustic prime movers. *Phys Lett A* 2006; 351: 268–273.
105. Penelet G, Gusev V, Lotton P, et al. Experimental and theoretical study of processes leading to a steady-state sound in annular thermoacoustic engines. *Phys Rev E* 2005; 72: 016625.
106. Lycklama A, Niejholt JA, Tijani MEH and Spoelstra S. Simulation of a travelling-wave thermoacoustic engine using computational fluid dynamics. *J Acoust Soc A* 2005; 118: 2265–2270.
107. Penelet G, Job S, Gusev V, et al. Dependence of sound amplification on temperature distribution in annular thermoacoustic engines. *Acta Acust* 2005; 91: 567–577.
108. Guedra M, Penelet G and Lotton P. Experimental and theoretical study of the dynamics of self-sustained oscillations in a standing wave thermoacoustic engine. *J Appl Phys* 2014; 115: 024504.
109. Yu Z, Jaworski AJ and Abdualil AS. Fishbone-like instability in a looped-tube thermoacoustic engine. *J Acoust Soc Am* 2010; 128: EL188.
110. Abdualil AS, Yu Z and Jaworski AJ. Non-linear phenomena occurring during the start-up process of a travelling-wave thermoacoustic engine. *Proc IMechE Part A, J Power Energy* 2012; 226: 822–836.
111. Lawn CJ. Development of a thermoacoustic travelling-wave engine. *Proc IMechE Part A, J Power Energy* 2013; 227: 498–514.
112. Yazaki T. Experimental observation of thermoacoustic turbulence and universal properties at the quasiperiodic transition to chaos. *Phys Rev E* 1993; 48: 1806–1818.
113. Penelet G and Biwa T. Synchronization of a thermoacoustic oscillator by an external sound source. *Am J Phys* 2013; 81: 290–297.
114. Li LKB and Juniper MP. Phase trapping and slipping in a forced hydrodynamically self-excited jet. *J Fluid Mech* 2013; 735: 1–11.
115. Unni VR, Prasaad MS, Ravi NT, et al. Experimental investigation of bifurcations in a thermoacoustic engine. *Int J Spray Combust Dyn* 2015; 7: 113–130.
116. Karpov S and Prosperetti A. A nonlinear model of thermoacoustic devices. *J Acoust Soc Am* 2002; 112: 1431–1444.
117. Hamilton MF, Ilinskii YA and Zabolotskay EA. Nonlinear two-dimensional model for thermoacoustic engines. *J Acoust Soc Am* 2002; 111: 2076–2086.
118. Biwa T, Takahashi T and Yazaki T. Observation of traveling thermoacoustic shock waves. *J Acoust Soc Am* 2011; 130: 3158–3161.
119. Olivier C, Penelet G, Poignand G, et al. Weakly nonlinear propagation in thermoacoustic engines: a numerical study of higher harmonics generation up to the appearance of shock waves. *Acust Acta Acust* 2015; 101: 1–9.
120. Shimizu D and Sugimoto N. Autonomous generation of a thermoacoustic solitary wave in an air-filled tube. *J Appl Phys* 2016; 120: 144901.
121. Palies P, Durox D, Schuller T, et al. Nonlinear combustion stability analysis based on the flame describing function applied to turbulent premixed swirling flames. *Combust Flame* 2011; 158: 1980–1991.
122. Moeck JP, Bourgouin J-F, Durox D, et al. Nonlinear interaction between a precessing vortex core and

- acoustic oscillations in a turbulent swirling flame. *Combust Flame* 2012; 159: 2650–2668.
123. Kim KT and Hochgreb S. Measurements of triggering and transient growth in a model lean-premixed gas turbine combustor. *Combust Flame* 2012; 159: 1215–1227.
 124. Lieuwen TC. Experimental investigation of limit-cycle oscillations in an unstable gas turbine combustor. *J Propulsion Power* 2002; 18: 61–67.
 125. Lieuwen TC and Neumeier Y. Nonlinear pressure-heat release transfer function measurements in a premixed combustor. *Proc Combust Inst* 2002; 20: 99–105.
 126. Matveev K and Culick FEC. A model for combustion instability involving vortex shedding. *Combust Sci Tech* 2003; 175: 1059–1083.
 127. Tulsyan B, Balasubramanian K and Sujith RI. Revisiting a model for combustion instability involving vortex shedding. *Combust Sci Tech* 2009; 181: 457–482.
 128. Wieczorek K, Sensiau C, Polifke W, et al. Assessing non-normal effects in thermoacoustic systems with mean flow. *Phys Fluids* 2011; 23: 107103.
 129. Kashinath K, Hemchandra S and Juniper M. Nonlinear thermoacoustics of ducted premixed flames: the influence of perturbation convection speed. *Combust Flame* 2013; 160: 2856–2865.
 130. Han X, Li J and Morgans AS. Prediction of combustion instability limit cycle oscillations by combining flame describing function simulations with a thermoacoustic network model. *Combust Flame* 2015; 162: 3632–3647.
 131. Noiray N, Durox D, Schuller T, et al. A unified framework for nonlinear combustion instability analysis based on the flame describing function. *J Fluid Mech* 2008; 615: 139–167.
 132. Boudy F, Durox D, Schuller T, et al. Nonlinear mode triggering in a multiple flame combustor. *Proc Combust Inst* 2011; 33: 1121–1128.
 133. Heckl M. A new perspective on the flame describing function of a matrix flame. *Int J Spray Combust Dyn* 2015; 7: 91–112.
 134. Pawar SA, Vishnu R, Vadivukkarasan M, et al. Intermittency route to combustion instability in a laboratory spray combustor. *J Eng Gas Turbine Power* 2016; 138: 041505.
 135. Hong JG, Oh KC, Lee UD, et al. Generation of low-frequency alternative flame behaviours in a lean premixed combustor. *Energy Fuels* 2008; 22: 3016–3021.
 136. Nair V, Thampi G and Sujith RI. Intermittency route to thermoacoustic instability in turbulent combustors. *J Fluid Mech* 2014; 756: 470–487.
 137. Domen S, Gotoda H, Kuriyama T, et al. Detection and prevention of blowout in a lean gas turbine model combustor using the concept of dynamical system theory. *Proc Combust Inst* 2015; 35: 3245–3253.
 138. Unni VR and Sujith RI. Flame dynamics during intermittency in a turbulent combustor. *Proc Combust Inst* 2017; 36: 3791–3798.
 139. Greatrix DR. Simulation of axial combustion instability development and suppression in solid rocket motors. *Int J Spray Combust Dyn* 2009; 1: 143–168.
 140. Yu Z, Saat FAZ and Jaworski AJ. Experimental testing of the flow resistance and thermal conductivity of porous materials for regenerators. In: *23rd international congress on refrigeration*, Prague, 21–26 August 2011.
 141. Guedra M, Bannwart FC, Penelet G, et al. Parameter estimation for the characterisation of thermoacoustic stacks and regenerators. *Appl Therm Eng* 2015; 80: 229–237.
 142. Yu Z and Jaworski AJ. Impact of acoustic impedance and flow resistance on the power output capacity of the regenerators in travelling-wave engines. *Energy Convers Manage* 2010; 51: 350–359.
 143. Yu Z, Li Q, Chen X, et al. Experimental investigation on a thermoacoustic engine having a looped tube and a resonator. *Cryogenics* 2005; 45: 566–571.
 144. Nouh MA, Arafa NM and Abdel Rahman E. Stack parameters effect on the performance of anharmonic resonator thermoacoustic heat engine. In: *3rd international conference on integrity, reliability and failure*, Porto, Portugal, 20–24 July 2009.
 145. Lawn CJ. Optimization of the loop of a travelling wave thermo-acoustic engine. In: *3rd international workshop on thermoacoustics*, University of Twente, Holland, 26–27 October 2015.
 146. Hatori H, Biwa T and Yazaki T. How to build a loaded thermoacoustic engine. *J Appl Phys* 2012; 111: 074905.
 147. Yahya SG, Mao X and Jaworski AJ. Two-stage looped-tube thermoacoustic cooler – design and preliminary testing. In: *Proceedings of the World Congress on Engineering 2016 Vol II*, London, UK, 29 June–1 July 2016.
 148. Bellucci V, Flohr P, Paschereit CO, et al. On the use of Helmholtz resonators for damping acoustic pulsations in industrial gas turbines. *ASME J Eng Gas Turbines Power* 2004; 126: 271–275.
 149. Tran N, Ducruix S and Schuller T. Passive control of the inlet acoustic boundary of a swirled burner at high amplitude combustion instabilities. *J Eng Gas Turbines Power* 2009; 131: 051502.
 150. Eldridge JD and Dowling AP. The absorption of axial acoustic waves by a perforated liner with bias flow. *J Fluid Mech* 2003; 485: 307–355.
 151. Lahiri C, Enghardt L, Bake F, et al. Establishment of a high quality database for the acoustic modelling of perforated liners. *J Eng Gas Turbine Power* 2011; 133: 0191503.
 152. Lahiri C and Bake F. A review of bias flow liners for acoustic damping in gas turbine combustors. *J Sound Vibr* 2017; 400: 564–605.
 153. Lawn CJ. Calculation of acoustic absorption in ducts with perforated liners. *Appl Acoust* 2015; 89: 211–221.
 154. Worth NA and Dawson JR. The effect of baffles on self-excited azimuthal modes in an annular combustor. *Proc Combust Inst* 2015; 35: 3283–3290.
 155. Parmentier J-F, Salas P, Wolf P, et al. A simple analytical model to study and control azimuthal instabilities in annular combustion chambers. *Combust Flame* 2012; 159: 2374–2387.
 156. Schadow KC and Gutmark E. Combustion instabilities related to vortex shedding in dump combustors and their passive control. *Prog Energy Combust Sci* 1992; 18: 117–132.

157. Bloxidge GJ, Dowling AP, Hooper N, et al. Active control of reheat buzz. *AIAA J* 1988; 26: 783–790.
158. Heckl MA. Active control of the noise from a Rijke tube. *J Sound Vibr* 1988; 124: 117–133.
159. Candel S. Combustion dynamics and control: progress and challenges. *Proc Combust Inst* 2002; 29: 1–28.
160. Sato H, Hayashi AK, Ikame M, et al. Active control of acoustically coupled pressure oscillation in lean pre-mixed combustor by secondary fuel injection. In: *Proceedings of the 5th international symposium smart control of turbulence*, Tokyo, 29 February–2 March 2004.
161. Bothien MR and Paschereit CO. Tuning of the acoustic boundary conditions of combustion test rigs with active control: extension to actuators with nonlinear response. *J Eng Gas Turbine Power* 2010; 132: 091503.
162. Olivier C, Penelet G, Poignand G, et al. Active control of thermoacoustic amplification in a thermo-acousto-electric engine. *J Appl Phys* 2014; 115: 174905.